

The Response of Embedded Strain Sensors in Concrete Beams Subjected to Thermal Loading

Yu Ge¹ (Corresponding Author), Mohammed Z. E. B. Elshafie², Samir Dirar³ and Campbell R. Middleton²

Abstract

A wide range of commercially available sensors are frequently used to record the response of civil engineering structures that may be subjected to unexpected loading scenarios, changes of environmental conditions or material deterioration. However, a common problem faced when using these sensors is to distinguish strain changes experienced by the structure due to a temperature change from strain changes that occur due to other causes. Temperature effects on strain sensors are usually accommodated by allowing for temperature effects (temperature compensation); however, there is limited research in the literature that investigates the performance of strain sensor measurements when subjected to temperature change. Understanding the temperature effect on strain sensors will greatly enhance the ability of civil engineers to monitor the performance of structural materials. In this paper, different types of commonly used and advanced strain sensors have been installed in a reinforced concrete beam to measure the thermal strain response of concrete under different temperature conditions. The experimental results demonstrated a 25-30% difference in strain measurements from the different sensors. It is shown in this paper that this difference is due to the combined effects of sensor inaccuracy, uncertainties related to the testing conditions and uncertainties associated with the temperature compensation methods.

Key words:

Concrete behaviour, Strain sensors, temperature compensation, Fibre Bragg Gratings, Brillouin backscattering, optical fibre sensors, vibrating wire strain gauges, thermal loading

¹ Ms. Yu Ge, 226/1 Acacia Place, Abbotsford, Victoria 3067, Australia. Tel: +61449859187, Email: yu.ge0427@gmail.com

² University of Cambridge, The Laing O'Rourke Centre for Construction Engineering and Technology, Department of Engineering, Trumpington Street, Cambridge, CB2 1PZ, United Kingdom

³ University of Birmingham, School of Civil Engineering, Edgbaston, Birmingham B15 2TT, United Kingdom

1. Introduction

Structural Health Monitoring (SHM) relies on the use of sensors to measure physical parameters. The strain change of structures is one of the most commonly assessed quantities in SHM to investigate the performance of structures under loading. There are three categories of commercially available strain sensors: (i) discrete strain sensors, (ii) quasi-distributed strain sensors and (iii) highly distributed strain sensors. Discrete sensors measure localised strain at the point where the sensor is installed while the highly distributed strain sensors measure the complete strain profile along the entire length of the sensor. Quasi-distributed strain sensors are discrete sensors connected in series. Measurements from these sensors are adversely affected by the surrounding environment such as temperature change which induces a thermal component in the sensor strain measurement. This is due to the different thermal expansion properties of the materials that constitute the sensor itself and the structural material in which the sensor is installed. Many civil engineering structures are subjected to repeated temperature changes on a very frequent basis hence it is important to understand how the thermal effects influence the strain measurements so that the mechanical strain induced by any unexpected loading scenarios or rapid material deterioration can be more accurately derived.

The effect of temperature on different sensors (conventional and advanced) has been researched by a number of researchers in the past. The following sections will briefly discuss some of the most significant research that has been done previously. Neild et al. (2005) conducted theoretical calculations to express the relationship between the measurements of Vibrating Wire Strain Gauges (VWSG) and the thermal deformation of a test specimen. Based on the results obtained, they argued that an unstrained VWSG (i.e. free from structural material deformations but under the same environmental conditions as the test specimen) should be used as a dummy gauge to compensate the temperature effect. However, they also found that if the sizes and geometries of the test specimens and the control samples were

1
2
3
4 significantly different, they would be affected differently by temperature. This may have a significant
5
6 implication, particularly in cases where such sensors are embedded in massive concrete structures like
7
8 bridges for example. Sreeshyarn et al. (2008) reported a temperature calibration factor of $2.19\mu\epsilon/^\circ\text{C}$ for
9
10 an embedded VWSG and $4.32\mu\epsilon/^\circ\text{C}$ for a surface mounted gauge on a concrete specimen. They
11
12 expressed concern that, due to the varied thermal expansion coefficient of concrete from one case to
13
14 another, an individual calibration test was required for each VWSG.
15
16
17
18
19
20

21 Recently developed measurement technologies, such as fibre optic sensors, have been used to measure
22
23 strain and/or temperature changes of structures whether embedded internally or attached externally.
24
25 The advantages of these sensors over conventional sensors (e.g. VWSGs) include: they are not affected
26
27 by electro-magnetic fields, longer sensing lengths and the potential to provide a long term reliable
28
29 monitoring solution (Chen et. al., 1994). Two types of fibre optic sensors are most commonly adopted in
30
31 practice: (a) the Fibre Bragg Grating sensors (FBG) and the distributed optical fibre cables (FO). The
32
33 former are quasi-distributed sensors where individual FBGs can be placed at numerous locations on one
34
35 cable (providing simultaneous multiple points sensing) while the latter have the advantage of providing
36
37 highly-distributed continuous strain profiles along the entire length of the optical fibre cables and are
38
39 believed to have potential for long term monitoring with less implementation costs (Hoult et al. 2009).
40
41 The particular FO technique discussed in this paper uses the Brillouin backscattering technique (Bao and
42
43 Chen, 2011). Published case studies in the literature where temperature compensation is discussed in
44
45 detail are very limited. Rodrigues et al. (2010) presented a study on FBG sensors where the FBG sensors
46
47 were initially fixed onto steel tubes before they were embedded in the concrete deck of the Lezíria
48
49 Bridge in Portugal. For temperature compensation in particular, the paper mentioned briefly that a
50
51 direct calculation could be applied with known temperature measurements at the location of the FBG
52
53 sensors, taking into account the characteristics of the FBGs and the material of the structure that was
54
55
56
57
58
59
60
61
62
63
64
65

1
2
3
4 being monitored. However, no further detail was given for the accuracy and reliability of measurements
5
6 after applying such a temperature compensation method. Mohamad (2008) discussed the use of
7
8 dummy temperature optical fibre cables alongside the active FO sensing cables to carry out temperature
9
10 compensation for distributed FO measurements. The design of the temperature optical fibre cable
11
12 allows the cables to be used for temperature compensation. The fibre core in the FO dummy
13
14 temperature cable can expand freely in a gel-filled tube and hence is isolated from any strains
15
16 transmitted to the outer sheath of the cable. The “temperature strain” measured by the temperature
17
18 cable is then subtracted from the total strain measured by the active FO sensing cable to calculate the
19
20 mechanical strain. Mohamad (2012) argued that using such a method is much cheaper and simpler than
21
22 other approaches, particularly when temperature coefficients relating to different types of optical fibres
23
24 can be easily estimated. Field case studies conducted recently (Webb, 2010 and Schwamb, 2010)
25
26 discussed the installation of FO temperature and strain cables in a number of pre-stressed concrete
27
28 bridge beams and cast in-situ concrete pile foundations at the Nine Wells Bridge near Cambridge, UK.
29
30 Schwamb (2010), who reported the pile foundation sensing results, pointed out that the accurate
31
32 interpretation of the measurements, including temperature compensation, is highly dependent on the
33
34 geometric alignment of the strain and temperature cables; a small mis-alignment of 5cm resulted in
35
36 significantly inaccurate results. Webb (2010) adopted the same temperature compensation method as
37
38 suggested by Mohamad (2012) and compared the temperature compensated FO measurements to the
39
40 theoretical strain prediction and found that the two were correlated well in larger scale.
41
42
43
44
45
46
47
48
49
50

51
52 In summary, SHM schemes have been used to monitor the performance of a number of civil engineering
53
54 structures, however, in most cases the sensors employed in these SHM schemes are likely to be
55
56 subjected to and affected by temperature changes. In most studies in the literature, measurements
57
58 from different independent instruments would normally be introduced to allow cross calibration and
59
60
61
62
63
64
65

1
2
3
4 comparison, however there is still little quantitative evidence available on the reliability of the different
5
6 sensors when subjected to temperature changes. Understanding the effect of the temperature changes
7
8 on the different strain sensors plays a significant role in understanding the performance of the
9
10 structures under conditions such as unexpected/extreme loading scenarios and rapid material
11
12 deterioration. The research presented in this paper provides quantitative information about the effect
13
14 of temperature on some of the most commonly used strain sensors such as the VWSGs and FBGs, as
15
16 well as some of the promising new strain sensors such as distributed FO sensors.
17
18
19
20
21
22

23 **2. Experiment design**

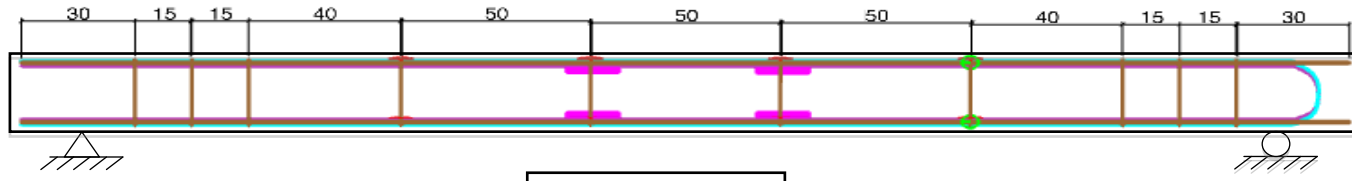
24
25
26
27 Since the vast majority of commonly used strain sensors are affected to some extent by temperature,
28
29 the reliability of their output measurements needs careful calibration and validation. Therefore, a
30
31 thorough study of the effect of temperature on strain measurements is needed. The research presented
32
33 in this paper examined the performance of strain sensors from two main perspectives:
34
35

- 36
37 1) How reliable is the sensor calibration and what is the accuracy of the measurements?
- 38
39 2) What role does temperature compensation play in the accuracy of measurements?
- 40
41
42
43

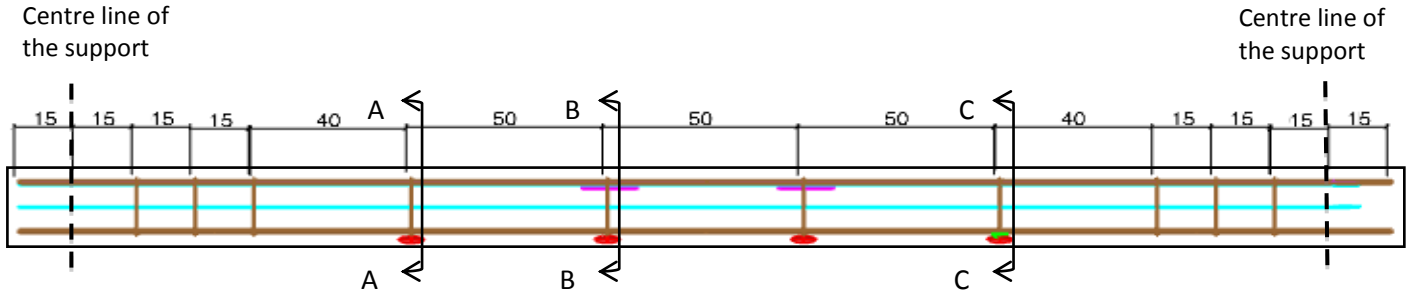
44
45 To investigate the questions above, an experimental programme was conducted in which a reinforced
46
47 concrete beam, instrumented with four types of strain sensors, was subjected to varied temperature
48
49 conditions without external mechanical loading. The beam was 3.5m in length with cross-section
50
51 dimensions of 25cm in depth and 20cm in width as shown in Figure 1. It had a cylinder compressive
52
53 strength of 32 MPa at 28 days. Four Grade 500B reinforcement steel bars with a diameter of 12mm
54
55 were used as longitudinal reinforcement while 8mm diameter shear links were used (at a spacing of
56
57 15cm towards the supports 50cm elsewhere) along the beam. The concrete cover was 20mm from the
58
59
60
61
62
63
64
65

1
2
3
4 surface of the beam to the surface of shear links. The beam was simply supported at each end with the
5
6 roller bearings allowing free expansion in the longitudinal direction. Four types of sensors were installed:
7
8 a conventional foil electrical resistance strain gauge (ERS), a Vibrating Wire Strain Gauge (VWSG), Fibre
9
10 Bragg Grating sensors (FBG) and distributed Brillouin backscattering optical fibre sensor (FO). The four
11
12 types of strain sensors were located so that the point sensors (ERS, VWSG and FBG) could be used to
13
14 compare results with those obtained with the distributed fibre optic sensor (FO). The location of the
15
16 different sensors in the beam is shown in Figure 1c and 1d. Temperatures inside the beam were
17
18 monitored by thermocouples (type K) and distributed optical fibre (FO) temperature cable.
19
20 Thermocouples were installed at the same locations as each of the discrete strain sensors (ERS, VWSG
21
22 and FBG) and also at the mid-height of the beam at a number of locations along the beam as shown in
23
24
25
26
27
28 Figure 2a and 2b.
29
30
31
32
33
34
35
36
37
38
39
40
41
42
43
44
45
46
47
48
49
50
51
52
53
54
55
56
57
58
59
60
61
62
63
64
65

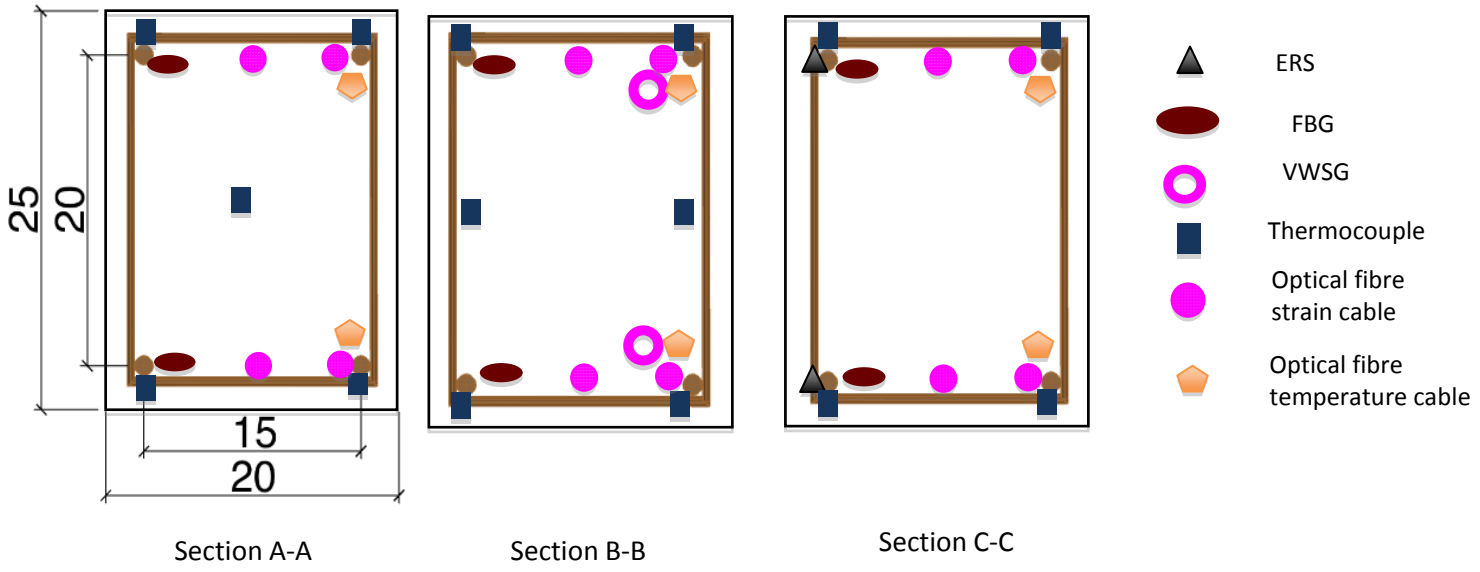
1
2
3
4
5
6
7
8
9
10
11
12
13
14
15
16
17
18
19
20
21
22
23
24
25
26
27
28
29
30
31
32
33
34
35
36
37
38
39
40
41
42
43
44
45
46
47
48
49









a) Elevation View



b) Top View



-  ERS
-  FBG
-  VWSG
-  Thermocouple
-  Optical fibre strain cable
-  Optical fibre temperature cable

c) Cross sections of beam

1
2
3
4
5
6
7
8
9
10
11
12
13
14
15
16
17
18
19
20
21
22
23
24
25
26
27
28
29
30
31
32
33
34
35
36
37
38
39
40
41
42
43
44
45
46
47
48
49

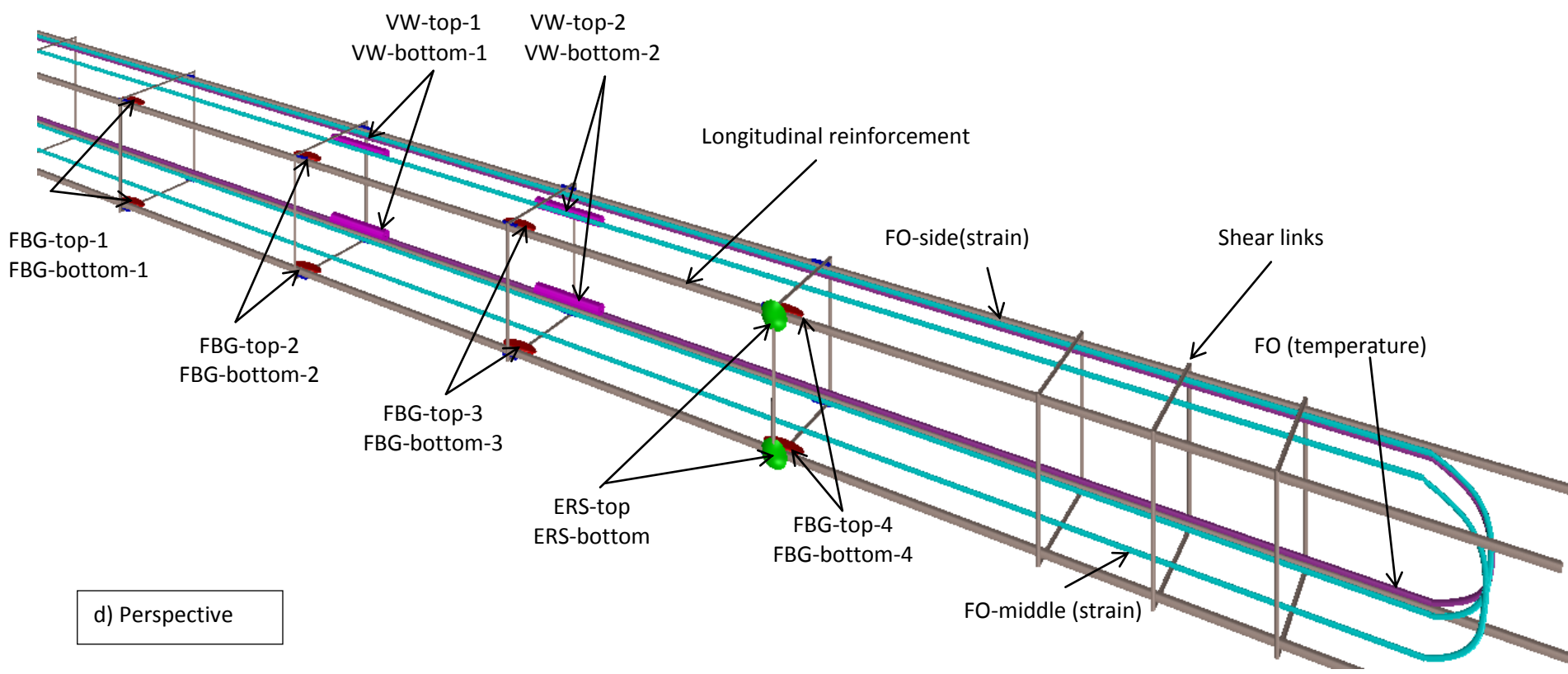
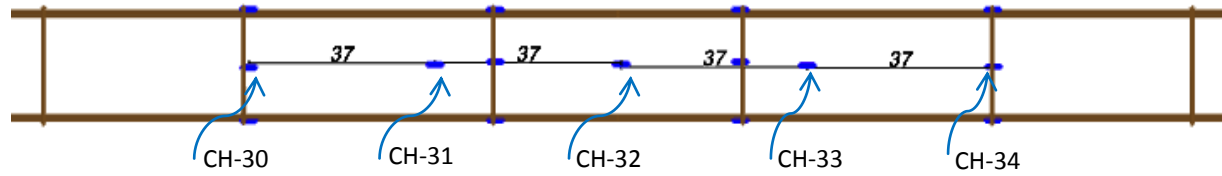
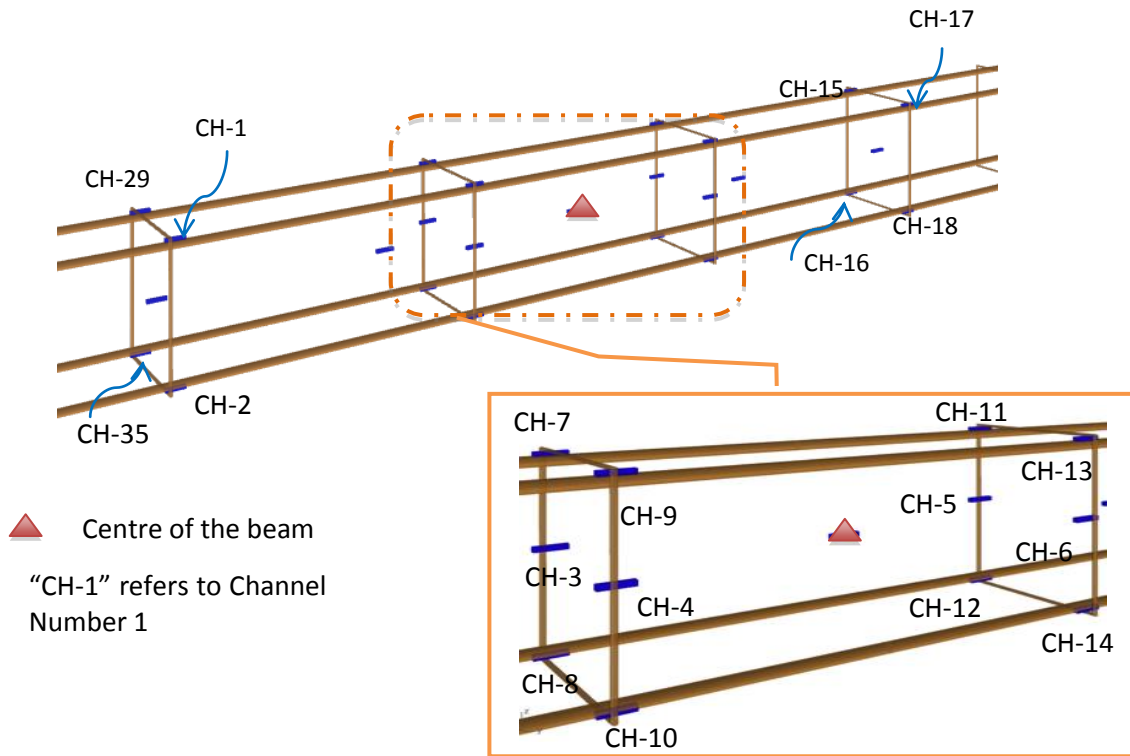


Figure 1 Schematic diagram of sensor instrumentation (All dimensions in CM)



a) Side elevation view of thermocouples locations (dimensions in 'cm')



b) Perspective view of thermocouples

Figure 2 Location of thermocouples

The experiment was divided into two parts; firstly, the whole beam was enclosed in an insulated box where all external surfaces of the beam were uniformly heated (from room temperature up to a maximum of 40°C in 1°C increments) as shown schematically in Figure 3a. In this case, the thermal strains measured from all instruments were expected to be the same given the beam was allowed to expand freely. In the second part of the experiment, the same concrete beam was used however, this time only the top surface of the beam was exposed to rising temperature inside the temperature box (Figure 3b), thus creating a temperature gradient through the depth of the beam. The bottom was

uncovered and exposed to ambient air temperature. The ends of the beam were wrapped with glass wool insulation which allows the beam to expand freely but prevents heat lost through ends. This part of the experiment was aimed at simulating the thermal loading experienced by bridge decks (where sunlight heats up the top surface of the bridge while the bottom surface is shaded).

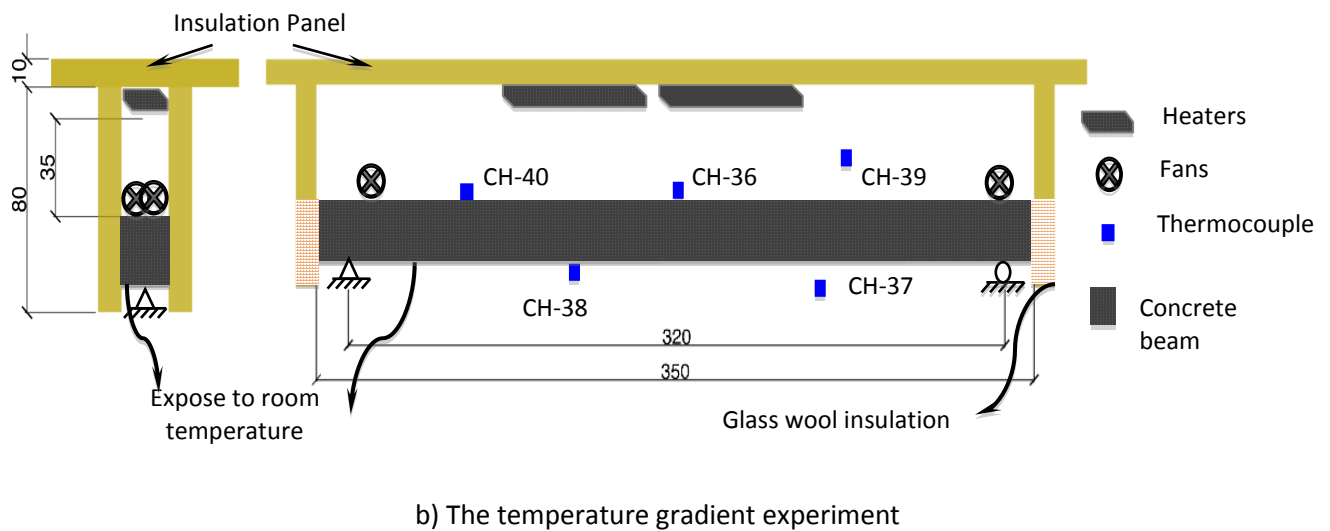
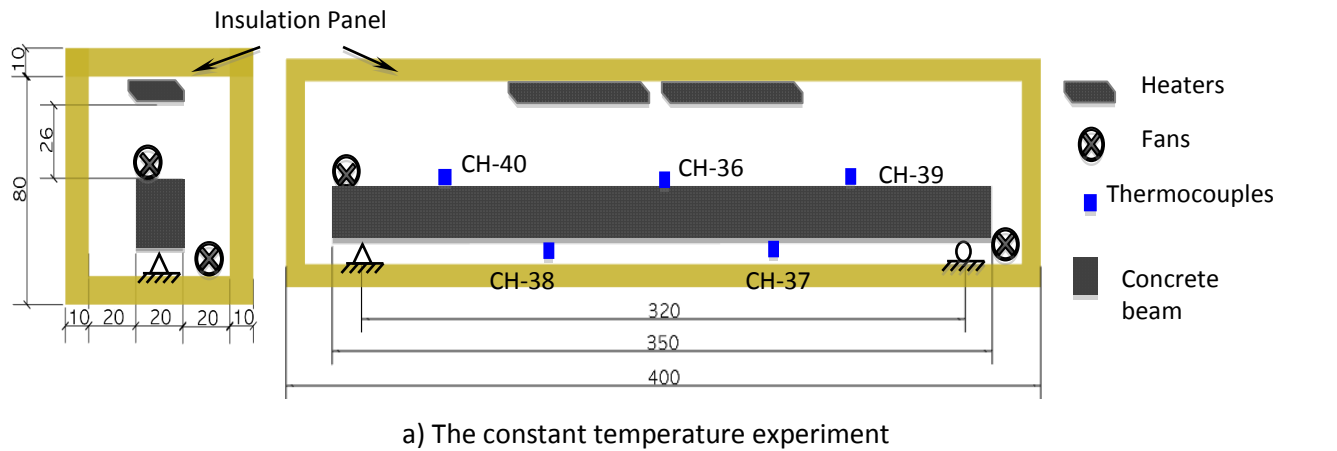


Figure 3 Schematic experimental setups (All dimensions are in CM)

Figure 4a and 4b show images of the experimental setup for the constant temperature test. Figure 4a shows an overview of the overall experimental setup while Figure 4b shows the different parts used to control the temperature imposed on the beam surfaces. Two 120 watt heaters were used to control the

1
2
3
4 temperature inside the experimental setup, with two fans used to circulate the air within the box. In
5
6 order to achieve uniform temperature conditions around the concrete beam, a number of preliminary
7
8 tests were conducted to optimise the location of the heaters and the fans; Figure 3a and 4b show their
9
10 final locations. Figure 5a, 5b and 5c show the experimental setup for the temperature gradient test. The
11
12 external fan shown in Figure 5a was used to increase the airflow at the bottom surface of the beam. This
13
14 is to ensure that a distinctive temperature gradient is created. Insulation was firmly attached to the two
15
16 sides of the beam to ensure only the top surface of the beam was affected by temperature change.
17
18
19
20
21 Figure 5c shows an image of the setup inside the insulated box.

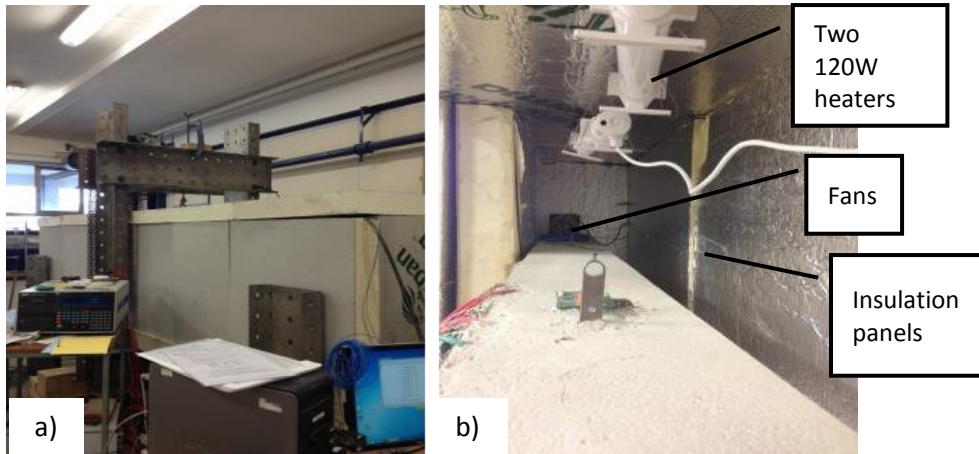


Figure 4 Experimental setup for constant temperature test

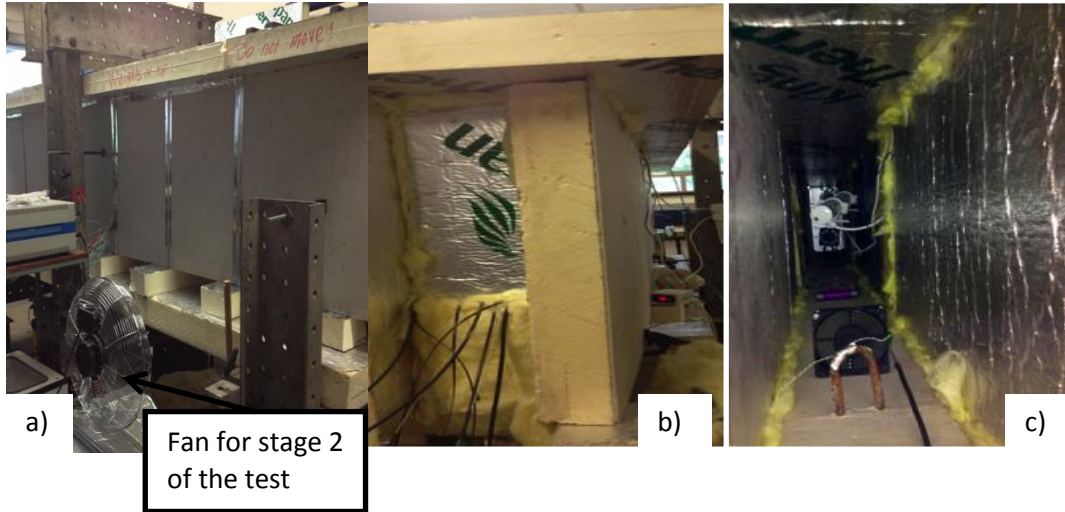


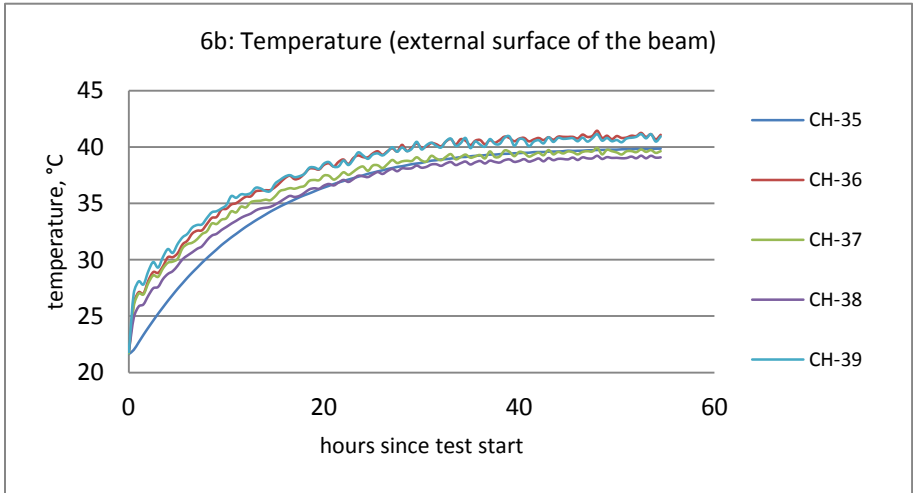
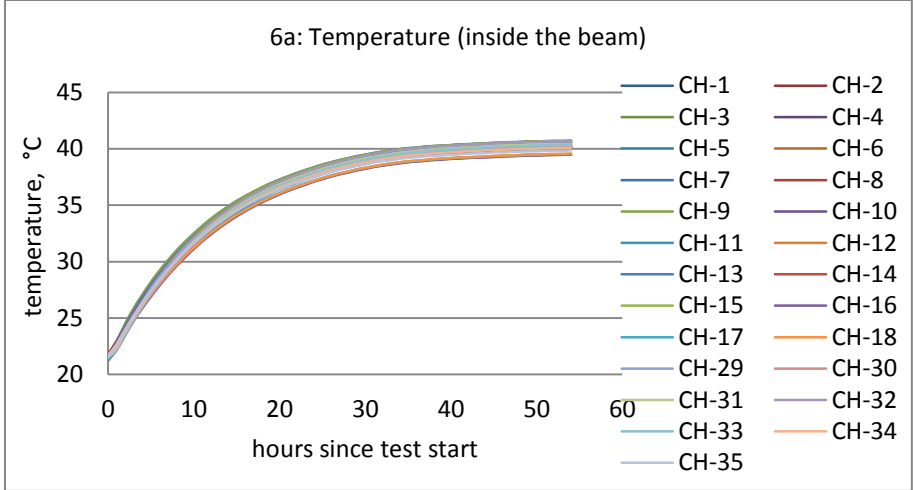
Figure 5 Experimental setup for temperature gradient test

3. Experimental Results

3.1. Constant temperature experiment

The temperature monitoring results at the locations shown in Figure 2 inside the concrete beam and at the locations shown in Figure 3a on the external surface of the beam are presented in Figure 6a and 6b. The consistency of temperature measurements along the beam span leads to the conclusion that the beam is exposed to uniformly distributed temperature all the time. Consequently, the mean temperature taken from all measurement points is representative of the temperature everywhere in the beam. The temperature difference between the core and the surroundings of the concrete beam became insignificant within 20 hours of the start of the test as shown in Figure 6c. The box temperature is the average reading of the external thermocouples shown in Figure 3a while the concrete temperature is the average reading of thermocouples show in Figure 2.

1
2
3
4
5
6
7
8
9
10
11
12
13
14
15
16
17
18
19
20
21
22
23
24
25
26
27
28
29
30
31
32
33
34
35
36
37
38
39
40
41
42
43
44
45
46
47
48
49
50
51
52
53
54
55
56
57
58
59
60
61
62
63
64
65



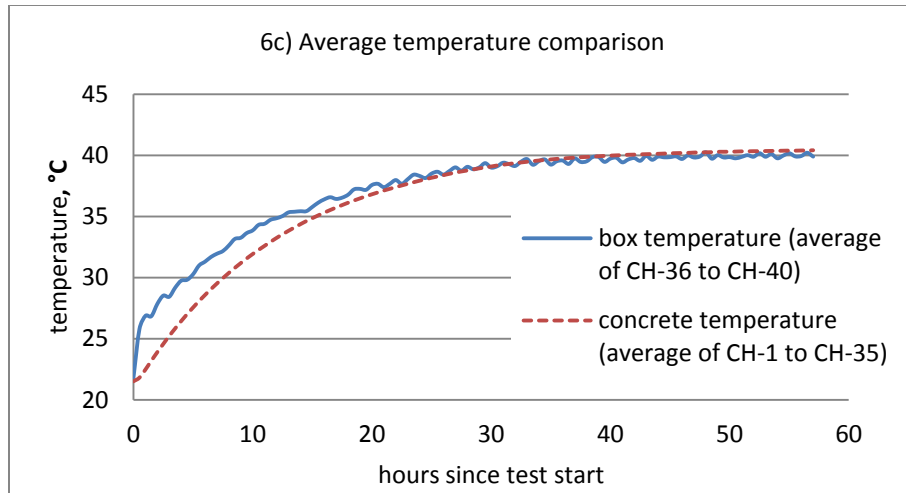
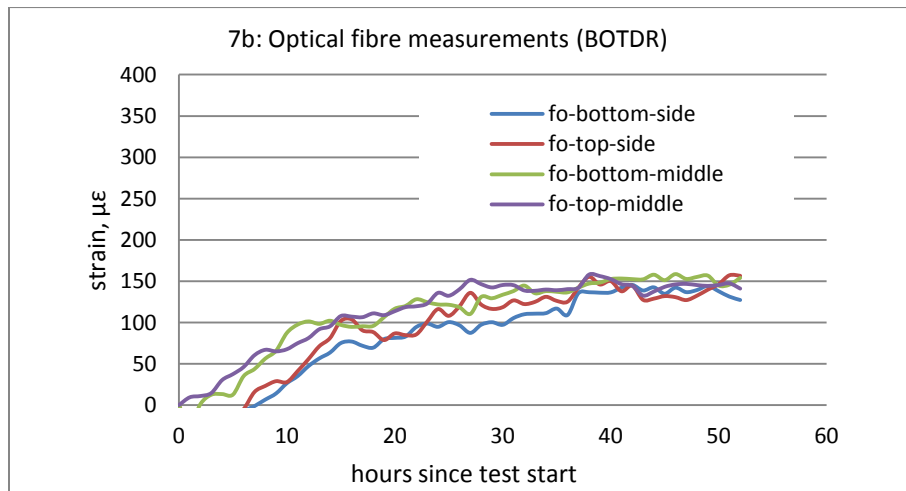
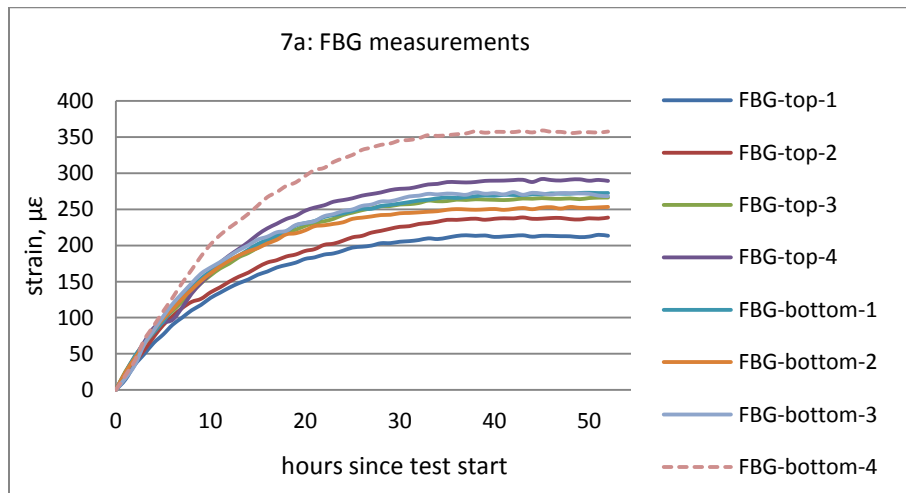
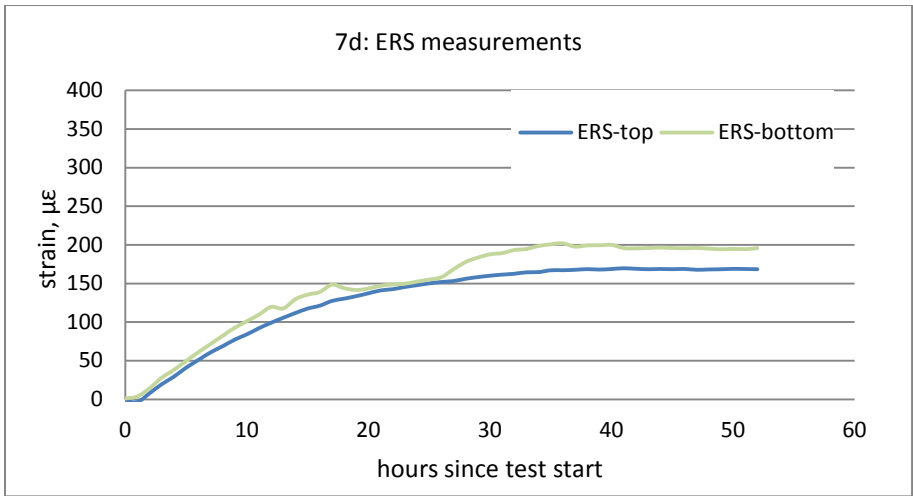
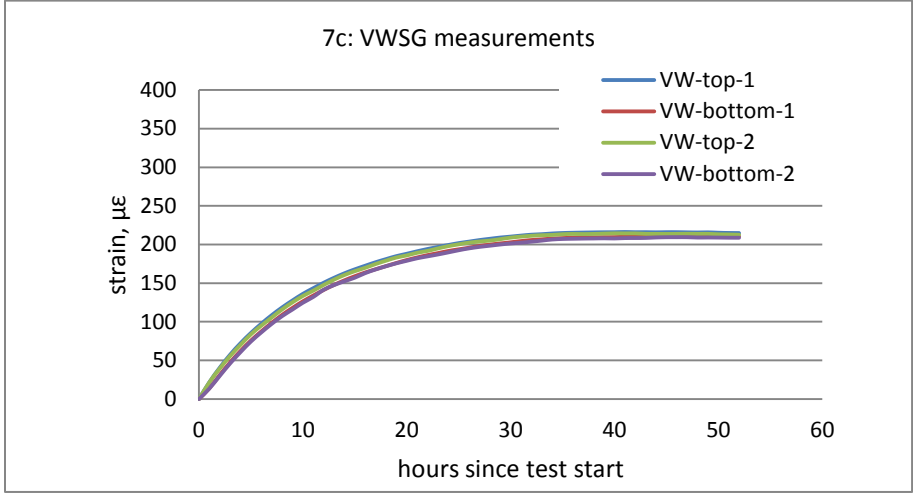


Figure 6 Temperature monitoring (Results from thermocouples)





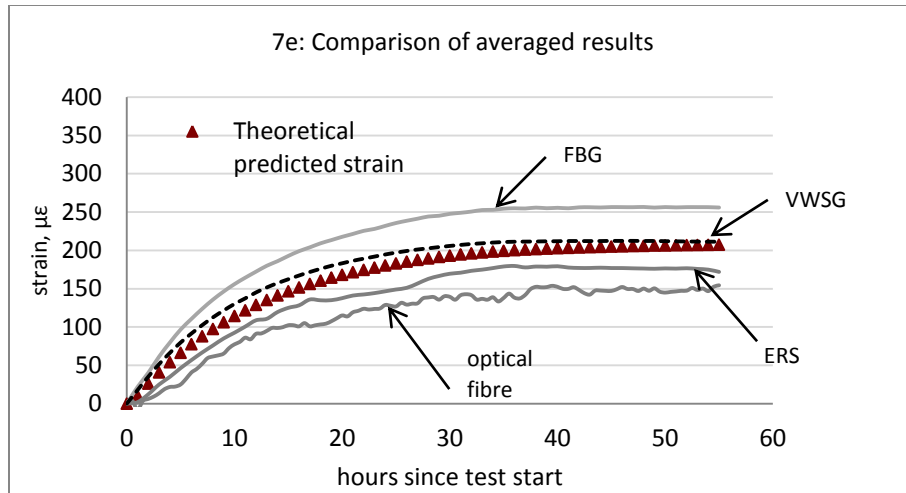


Figure 7 Temperature compensated strain results

Figure 7a to 7d show the results from each of the strain measurements after compensating for temperature effects from the different sensors. Temperature effects were considered by adopting a temperature calibration factor. This factor was different from one type of sensor to another and in this experiment was mainly obtained from manufacturers. It is clear from the plots that there is relatively little difference (maximum of 15%) (apart from the FBG sensors which will be discussed in later sections) between the measurements of the different sensors of the same type, therefore the measurements of each sensor type can be represented by an average line for better comparison. Figure 7e plots the average values from the different sensor types together with the theoretical predictions of strain obtained (using a thermal expansion coefficient of concrete of $11\mu\epsilon/^\circ\text{C}$ (Neville, 1997)). The average FBG and VWSG measurements produced a smooth curve when plotted against time whereas the other sensors showed more fluctuations in the results. FO sensors, which had a longer measurement time (around 20 minutes per measurement compared to instantaneous measurements for the other sensors), show larger fluctuations suggesting that FO sensors are unlikely to give stable measurements under rapidly changing temperature conditions. The results presented in Figure 7e were filtered measurements, in which a moving average was applied over each 10 data points along the length. The

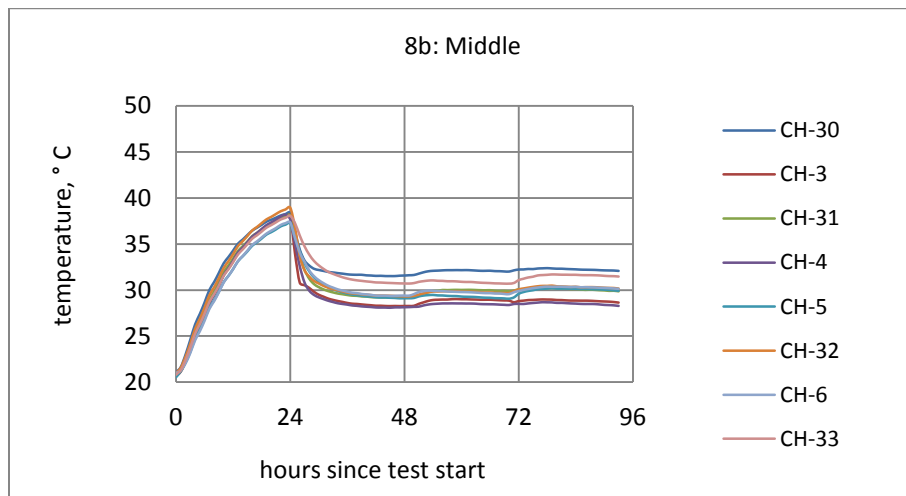
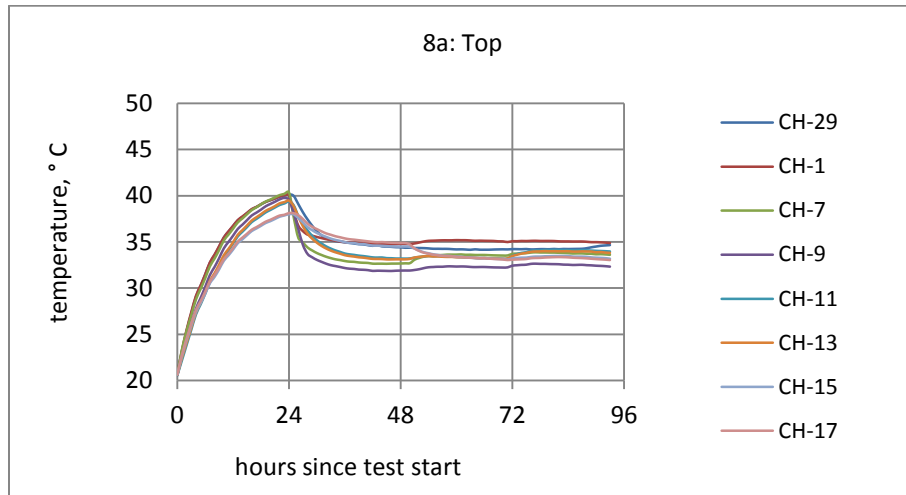
1
2
3
4 strain measurements from all the sensors, after allowing for temperature effects, were within $\pm 25\%$
5
6 from the calculated concrete thermal strains.
7
8
9

10 11 **3.2. Temperature gradient experiment**

12 Temperature measurements from the thermocouples inside the beam (Figure 2 taken over a 95-hour
13
14 period are presented in Figure 8a to 8c. These show that the thermocouple measurements at the same
15
16 levels (same depths through the beam) are very consistent hence average values can represent the
17
18 temperature at different levels. The lines labeled as Concrete-top, Concrete-middle and
19
20 Concrete-bottom in Figure 8d refer to the average measurements from all the thermocouples at the top,
21
22 middle and bottom parts of the beam respectively. For this part of the experiment, the beam was
23
24 subjected to two heating processes in two stages. In stage 1, the air temperature inside the box was
25
26 heated up to a maximum of 46°C in 10 hours with the top surface temperature of the beam reaching a
27
28 maximum of 42°C (Figure 8d). In stage 2, the air temperature inside the box was kept at 46°C with the
29
30 external fan (shown in Figure 5a) on the underside switched on (24 hours after the test had been started)
31
32 to accelerate the airflow at the bottom surface of the beam in order to maximise the temperature
33
34 difference between the top and bottom surfaces of the beam. The process finally stabilised at
35
36 approximately 14°C difference between the top and bottom surfaces and about 7°C difference between
37
38 the top and bottom reinforcement layers inside the concrete beam.
39
40
41
42
43
44
45

46 The strain results obtained from sensors are shown in Figure 9 for the top, middle and bottom parts of
47
48 the beam respectively. Each line shown in Figure 9a and 9b is the average plot for all the sensors of the
49
50 same type; the strain measurements obtained from the same type sensors at the same depth in the
51
52 beam were very consistent. The theoretical strain for the concrete was again calculated assuming a
53
54 thermal expansion coefficient of $11\mu\epsilon/^{\circ}\text{C}$. Despite the sensitivity of each sensor, the difference in
55
56 conductivity of concrete and steel created a complicated heat conduction process in the bottom part of
57
58
59
60
61
62
63
64
65

1
2
3
4 the beam, which caused a bigger variation in the bottom measurements (30%) as shown in Figure 9b.
5
6 The results from FO, which requires longer sensing time, can clearly demonstrate the unavoidable effect
7
8 of temperature changes on strain measurements. The measurements from the ERS in particular were 50%
9
10 lower than measurements from other sensors and the theoretical values. This could be due to ERS creep
11
12 lower than measurements from other sensors and the theoretical values. This could be due to ERS creep
13
14 when subjected to increasing temperature.
15
16
17
18
19
20
21
22
23
24
25
26
27
28
29
30
31
32
33
34
35
36
37
38
39
40
41
42
43
44
45
46
47
48
49
50
51
52
53
54
55
56
57
58
59
60
61
62
63
64
65



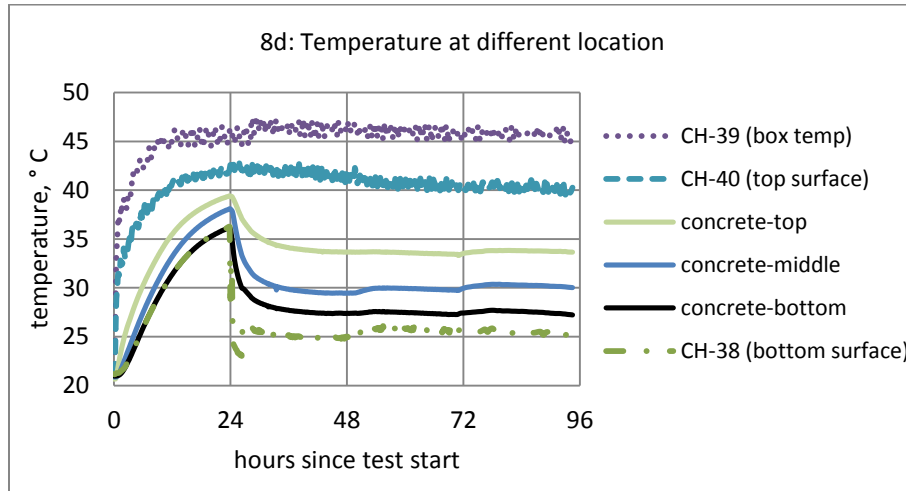
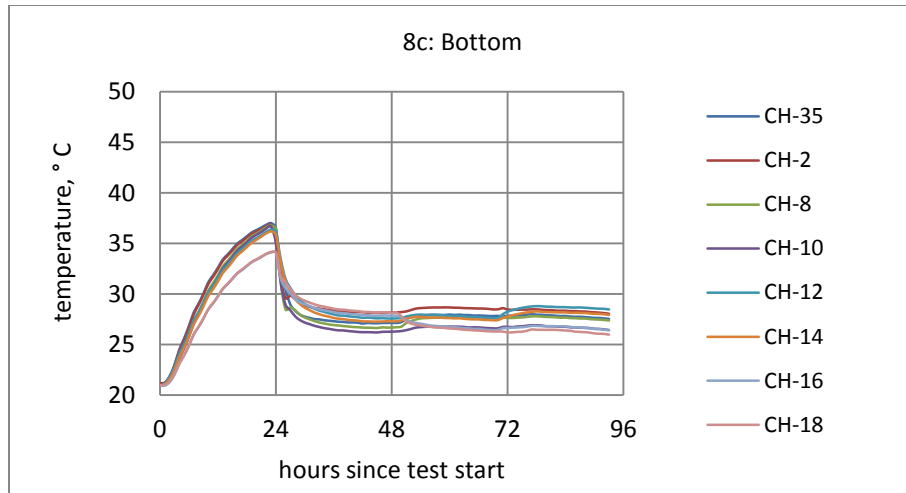


Figure 8 Temperature gradient through beam depth

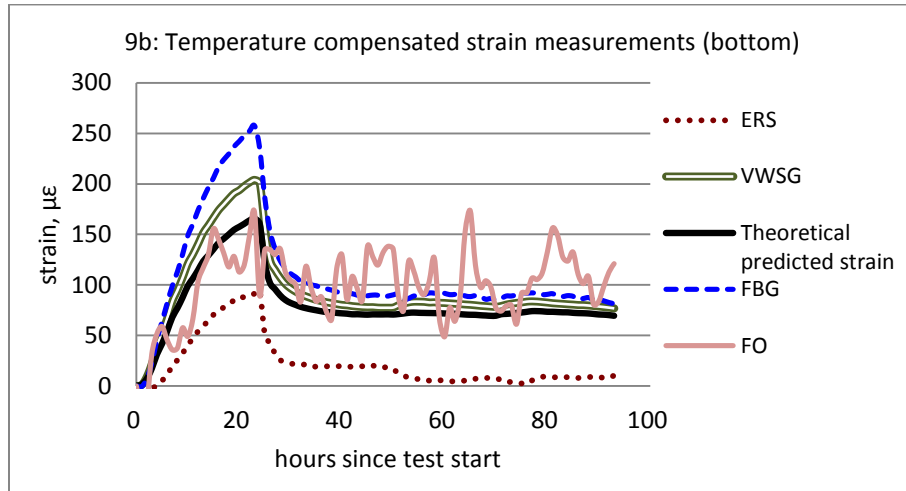
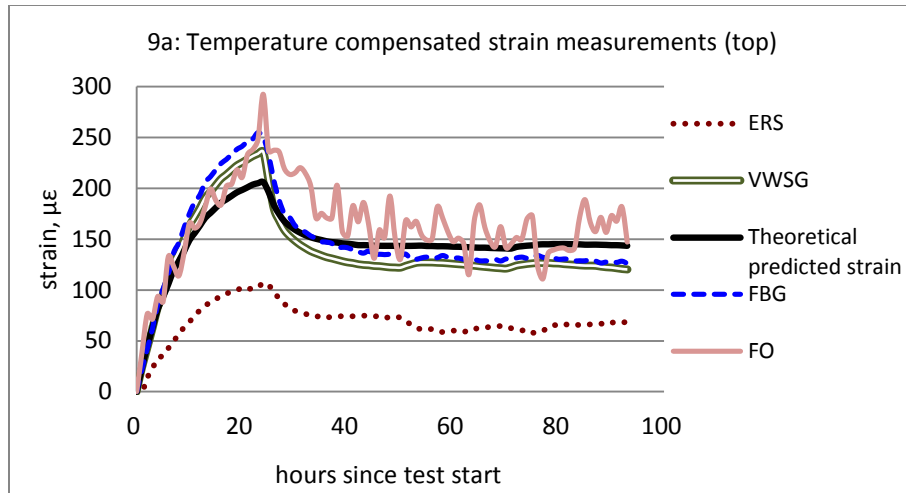


Figure 9 Strain measurements of instruments inside the concrete beam subjected to dynamic temperature environment

4. Discussion

4.1. Fibre Bragg Gratings (FBGs)

FBGs are essentially reflectors built inside the core of an optical fiber. The reflectors are made by permanently altering the refractive index of the core. Each FBG reflects a certain narrow slice of

1
2
3
4 spectrum. Such slices typically have a smooth Gaussian shape; the centre (i.e., top) of the reflected
5
6 Gaussian peak is what is used to make measurements. The FBG's peak shifts (to a higher or lower center
7
8 wavelength) when either the fiber is strained or its temperature changes.
9

10
11
12
13
14 The measurements obtained from the sensor labeled as "FBG-bottom-4" (the bottom sensor on the
15
16 right as shown in Figure 1d) showed a significant variation (about $100\mu\epsilon$) from all the others at the
17
18 maximum temperature to which the concrete beam was subjected (Figure 10a). Looking into the
19
20 spectrum response of this particular FBG, three peaks were noticed for measurements above 32°C , so
21
22 the analyser tracked different peaks at different times leading to large measurements.
23
24 Measurements from the rest of FBG sensors varied by approximately 10% from the average (From
25
26 Figure 10b the average is $275\mu\epsilon \pm 48\mu\epsilon$). The linear nature of the plots in Figure 10a and 10b may
27
28 suggest that this variation between the FBG measurements is due to the effect of using inaccurate strain
29
30 calibration coefficients, however, other factors such as sensor installation effects (bonding between the
31
32 sensor and the steel reinforcement) and localised effects (effect of the localised concrete strains on the
33
34 sensor) could have also influenced the measurements. Temperature compensation is conducted by
35
36 using a temperature calibration factor (also called the thermal-optical constant) which relates the shift
37
38 in wavelength of the Gaussian's peak to temperature change (Kreuze,2013). For a given temperature
39
40 change the corresponding wavelength shift is calculated and subtracted from the total shift. In Figure
41
42 10b, which shows the temperature compensated FBG strain measurements, inconsistency between the
43
44 FBG sensors is observed; a number of factors might have caused such variation.
45
46
47
48
49
50
51
52

53 1) The resolution of the recorded temperature measurements (temperature measurement
54
55 resolution): In this case, approximately $\pm 8\mu\epsilon$ difference could have been caused due to the $\pm 1^{\circ}\text{C}$
56
57 thermocouple resolution.
58
59
60
61
62

1
2
3
4 2) The temperature calibration of the FBG sensors: standard practice is to apply a conversion
5 coefficient to the frequency shift output from the sensors. Manufacturers typically use a single
6 conversion coefficient for all the sensors supplied (0.017nanometer/°C for the FBGs used in this
7 research). However, thermal calibration tests performed by the authors (described in more detail
8 later) found that a difference of up to $\pm 2\%$ (4% variation in total) could be measured between
9 individual sensors on the same cable when subjected to the same temperature change. According
10 to the FBG manufacturer’s datasheet, a strain of magnitude $1\mu\epsilon$ causes a peak wavelength shift of
11 1.213 picometer, therefore, at 42°C , the total 4% variation equates to about $24\mu\epsilon$ ($\pm 12\mu\epsilon$).
12
13

14 3) The two factors above could account for $28\mu\epsilon$ of a total discrepancy of $48\mu\epsilon$ discrepancy
15 observed in Figure 10b. The other $20\mu\epsilon$ could be attributed to other effects like the bonding
16 between the FBG sensors, the steel reinforcement and the surrounding concrete; normally
17 assumed to be the same for all the sensors, however, in practice it is not possible to verify that this
18 is the case. In addition, the concrete surrounding the sensors is assumed to behave homogenously
19 throughout but in practice the concrete will have minor variations along the beam resulting in small
20 different bond characteristics with the FBG sensor and the steel.
21
22
23
24
25
26
27
28
29
30
31
32
33
34
35
36
37
38
39
40
41

42 Measurements of FBG sensors from stage 1 of the temperature gradient test (as detailed in Section 3.2)
43 after temperature compensation are shown in Figure 11. The graph shows that the FBG sensors did not
44 pick up the strain difference due to the 3°C temperature gradient, recorded 24 hours after the start of
45 the test, between the top and bottom reinforcement layers (see Figure 8d). Such a temperature
46 gradient corresponds, in theory, to about $30\mu\epsilon$ strain difference; it is interesting to note that the
47 manufacturer of the FBGs claims a $1\sim 2\mu\epsilon$ strain resolution.
48
49
50
51
52
53
54
55
56
57
58
59
60
61
62
63
64
65

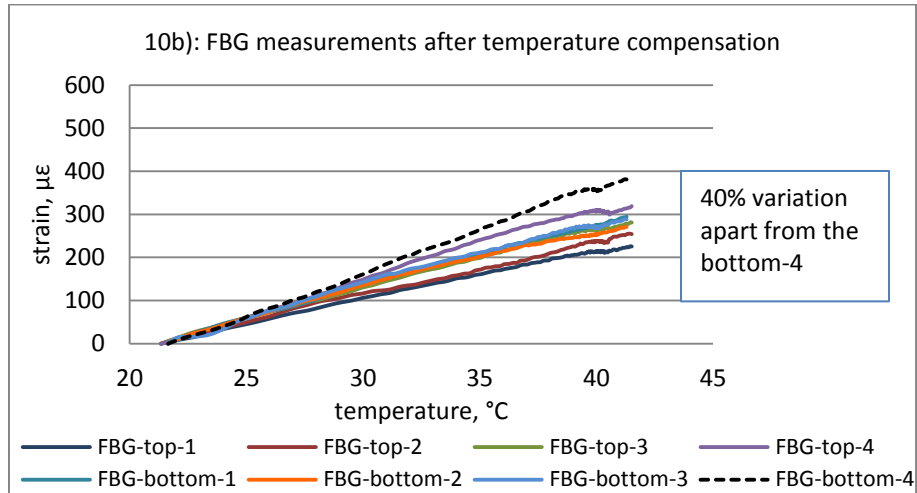
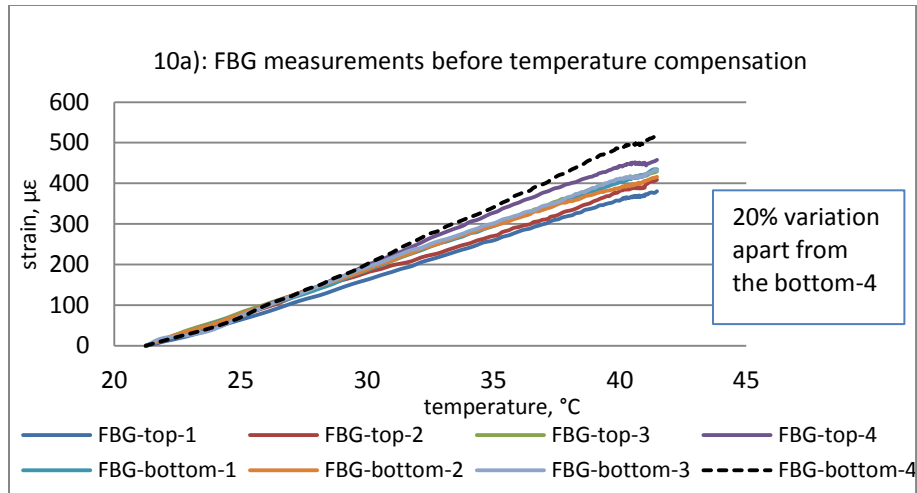


Figure 10 Results of FBG sensors from the constant temperature test

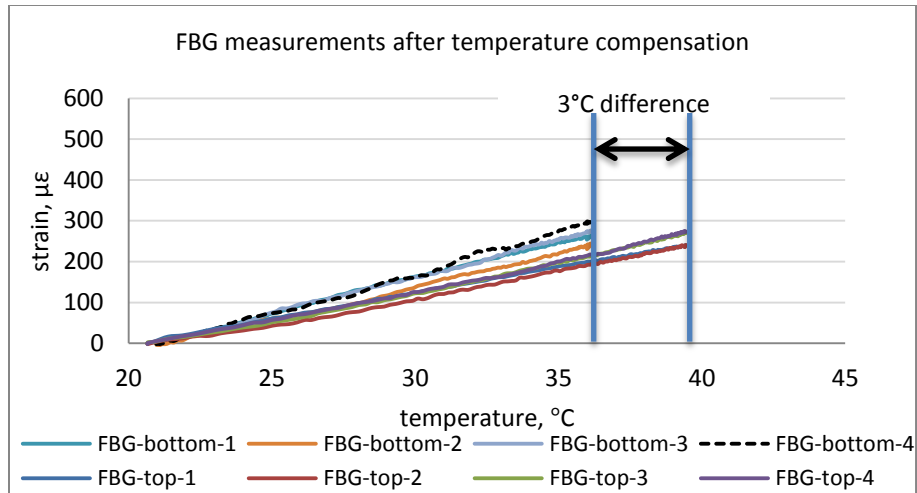


Figure 11 FBG strain measurements from the temperature gradient test (stage 1) after temperature compensation

To better understand the consistency of FBG sensors strain measurements, a temperature calibration test was also carried out by placing a test cable (five FBG sensors manufactured on a single cable) into a water tank as shown in Figure 12. The water temperature was controlled by a heater and measured by three different thermocouples at different locations as shown in the figure. Data from the fourth sensor (FBG-4) were excluded because as temperature increased, it experienced data loss. This might be because the sensor was located close to the heater and the fan (used to distribute heat around), which caused the sensor experienced unusual strain changes. The results, plotted in Figure 13, show a 4% difference between the sensors when subjected to the same temperature change (at 42°C this equates to approximately 24μϵ). This inconsistency reveals that applying an average temperature coefficient to different FBG sensors is insufficient to obtain reliable measurements.

1
2
3
4
5
6
7
8
9
10
11
12
13
14
15
16
17
18
19
20
21
22
23
24
25
26
27
28
29
30
31
32
33
34
35
36
37
38
39
40
41
42
43
44
45
46
47
48
49
50
51
52
53
54
55
56
57
58
59
60
61
62
63
64
65

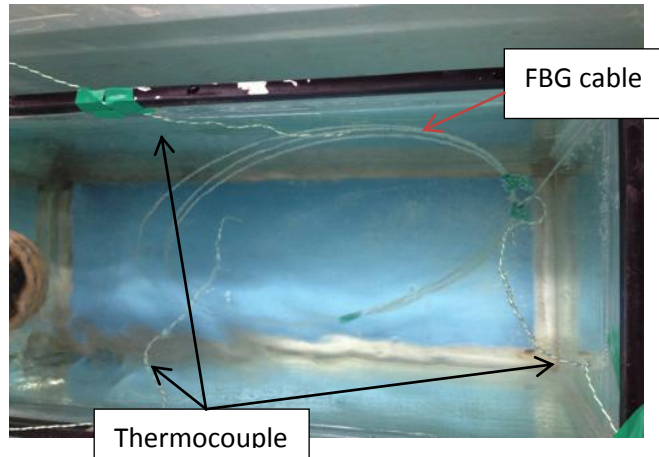


Figure 12 FBG temperature test setup

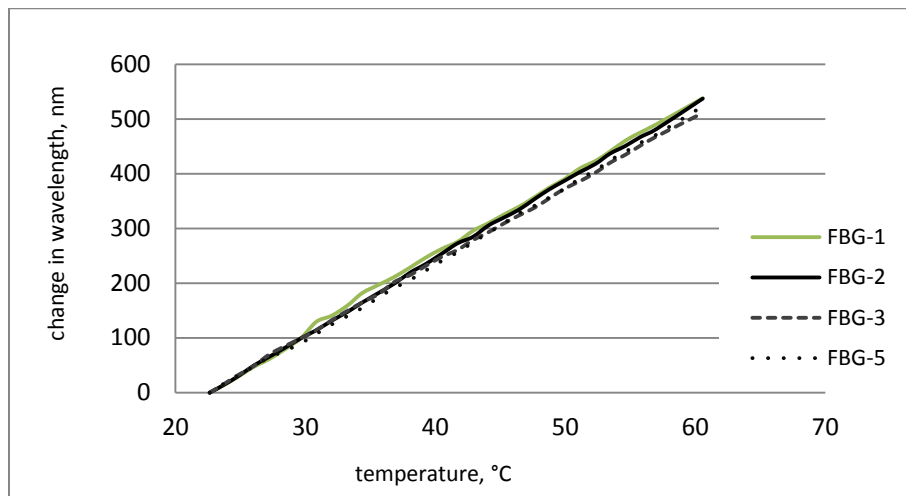


Figure 13 Temperature test results of FBG sensors

4.2. Vibrating wire strain gauges (VWSG)

Compared to the FBG sensors, measurements from the VWSGs exhibited very good consistency throughout all the tests. In particular, for the temperature gradient test, VWSG results clearly indicate the strain difference (that is induced by the temperature difference between top and bottom of the beam as shown in Figure 15, which is not captured by FBG sensors). The raw results from VWSGs had a nonlinear negative relationship between measured strain and temperature as shown in Figure 14. The

1
2
3
4 thermal output of VWSGs is induced by the difference in expansion of the steel wire in the gauge and
5
6 the concrete. The thermal output is calculated as follows (with known temperature and thermal
7
8 expansion coefficient of steel) (Geokon-VWSG Manual):
9

$$\varepsilon = 3.304 \times 10^{-3} B(f_1^2 - f_0^2) + (T_1 - T_0)C_1 \quad \text{Equation 1}$$

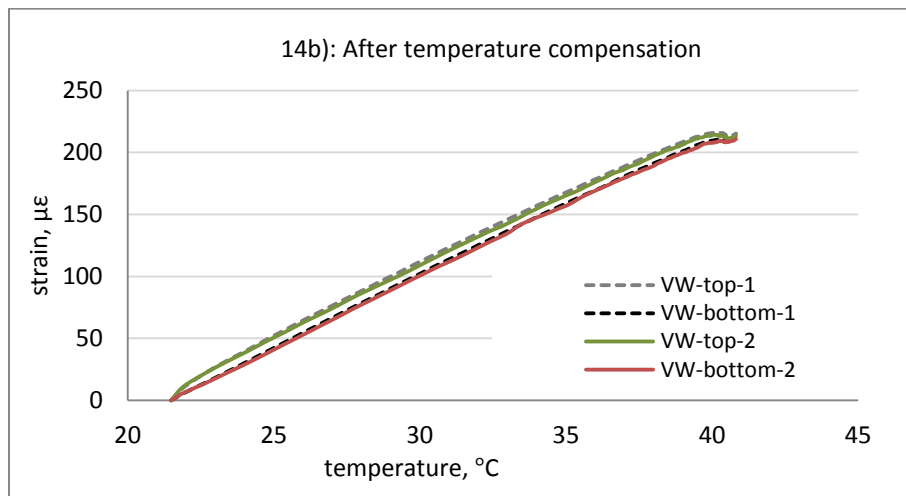
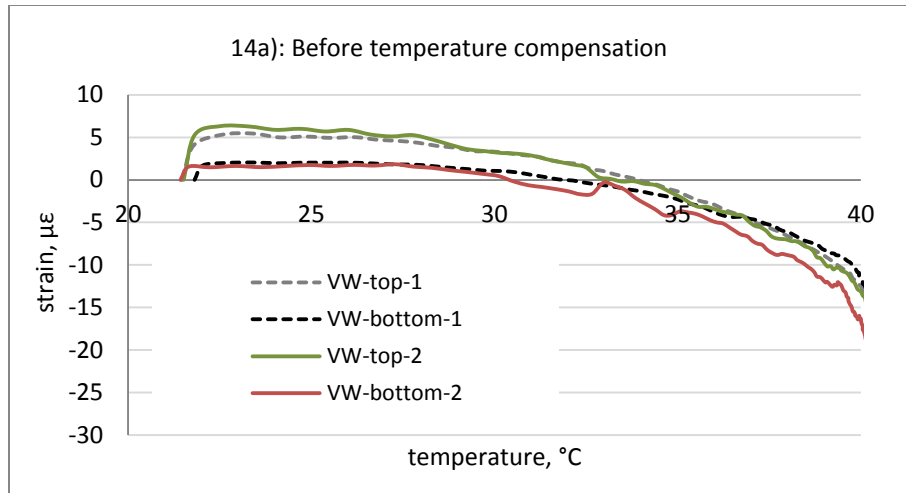
10
11
12
13
14 Where B: the batch calibration factor provided by the VWSG manufacturer

15
16 f_1, f_0 : final and initial frequencies

17
18 T_1, T_0 : final and initial temperatures

19
20 C_1 : thermal expansion coefficient of steel (=12.2 $\mu\epsilon/^\circ\text{C}$)
21
22
23
24
25

26 Compared to the total raw strain recorded by the VWSG, the steel thermal strain is significantly large
27
28 and therefore dominates the shape of the graph of temperature compensated measurements as shown
29
30 in Figure 14b and Figure 15. Even though the linearity in response is achieved by conducting a
31
32 theoretical calculation, the good agreement between estimated concrete strain and the actual
33
34 measurements provides strong evidence that the standard temperature compensation method
35
36 (Equation 1 above) is adequate. A maximum discrepancy of about 10 $\mu\epsilon$ is noticed in Figure 14b; this is
37
38 well within the uncertainty due to the temperature resolution measurement of $\pm 1^\circ\text{C}$. The VWGSs are
39
40 fixed mechanically to the steel bars, so installation and bonding issues are not expected to have any
41
42 significant influence.
43
44
45
46
47
48
49
50
51
52
53
54
55
56
57
58
59
60
61
62
63
64
65



41 **Figure 14 Results of VWSG from the constant temperature test**

42
43
44
45
46
47
48
49
50
51
52
53
54
55
56
57
58
59
60
61
62
63
64
65

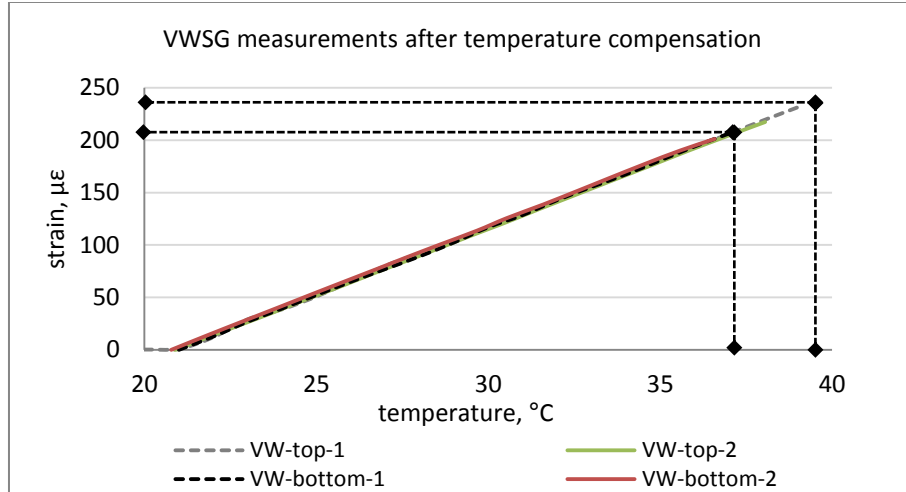


Figure 15 VWSG strain measurements from the temperature gradient test (stage 1) after temperature compensation

4.3. Distributed optical fibre sensing cables

Fibre optic strain sensing technology capitalises the capability of light wave to travel along the entire length of a cable and the strain dependency frequency shift of the backscattered light to provide a continuous and distributed strain sensing solution (Mohamad, 2008). Through the principle of Brillouin Optical Time Domain Reflectometry (BOTDR), when light passes through the fibre optic cables, a small amount of signal will be reflected back to the source as backscattered light. These may come in the form of Rayleigh, Brillouin and Raman backscattering. Within Brillouin backscattering, the peak Brillouin frequency experiences a shift when strain is induced. A linear correlation exists between the frequency shift and strain of the fibre optic cable. With the known time it takes for the backscattered signal to return to source, distance can be measured to a particular point of which the frequency shift or strain was measured. This effectively transforms the fibre optic cable to be the sensor itself, thus providing a continuous strain profile along its entire length. As shown in Figure 1, the beam was instrumented using fibre optic cables at varies locations along the beam. For strain measurement, the Fujikura Reinforced

1
2
3
4 Ribbon Cable (JBT-03813) was used; the nylon coating and the inner glass cores are fixed together
5
6 (known as tight-buffered) to ensure that the strain applied on the outer nylon sheath is transmitted into
7
8 the cores. For temperature measurement, the standard loose-tube Unitube cable was used; the optical
9
10 cores in this cable are surrounded by a gel and so the strain applied on the outer sheath does not get
11
12 transmitted into the cores. Figure 16 shows the cross-sections of the two cables.
13
14

15
16 Comparison of temperature profiles obtained by the distributed Unitube fibre optic temperature cable
17
18 with the discrete temperature measurements obtained by the thermocouples (locations of
19
20 thermocouples shown in Figure 17) is shown in Figure 18 at different times during the test. The BOTDR
21
22 measured strain from the Unitube cables are converted into temperature by using the conversion factor
23
24 $23.67\mu\epsilon/^\circ\text{C}$ (Mohamad et al (2014)). From the constant temperature test where heat is gently conducted
25
26 through the beam, as expected, temperature increased very quickly at beginning, corresponding to
27
28 bigger jumps from one profile to another. Comparing FO measured temperature with the thermocouple
29
30 readings, an average 2°C difference was observed (Figure 18a). This is perhaps not surprising given that
31
32 the resolution of the fibre optic measurement device using the Unitube cable is about $\pm 100\mu\epsilon$ which
33
34 translates to about 4°C uncertainty in temperature measurement. This is in addition to the $\pm 1^\circ\text{C}$
35
36 uncertainty associated with the temperature measurement. Mohamad et al. (2014) embedded a fibre
37
38 optic Unitube cable and thermocouples inside a concrete beam to measure the temperature change
39
40 (using the two different sensors simultaneously) during the curing process following casting of the beam.
41
42 When compared, the fibre optic cable measurements and the thermocouples' measurements had a
43
44 difference of about 1.5°C ; this is similar to what was observed in the tests reported in this paper.
45
46
47
48
49
50
51
52
53
54
55
56
57
58
59
60
61
62
63
64
65

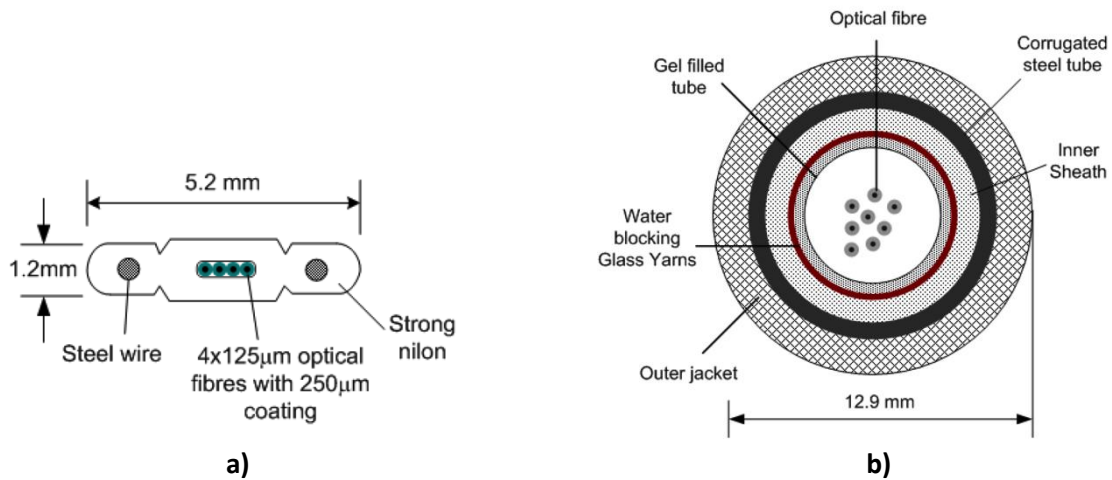


Figure 16 (a) The Fujikura Reinforced Ribbon cable and (b) The Unitube cable

For the temperature gradient test where heat is conducted from the top to the bottom of the beam, Figure 18b shows the results at the start of the temperature gradient test as well as at 4, 10 and 24 hours after the test start (24hours corresponds to the end of Stage 1). The FO temperature measurements, under such a relatively dynamic temperature environment, had about 5°C difference when compared to the thermocouples. Distributed FO temperature measurements are not sufficient to provide accurate local temperature information. However with the ability to provide a continuous temperature profile along the cable length, FO temperature cables are very useful in assisting engineers to assess the general temperature condition of structures. Figure 18b shows that the sensors in the middle of the beam measured slightly lower temperatures in comparisons the outer ones. The underside of the beam had better air flow in the middle compared to the ends due to the experimental setup required to hold the beam and insulation around it. This could explain why the middle was slightly lower in temperature compared to the sides.

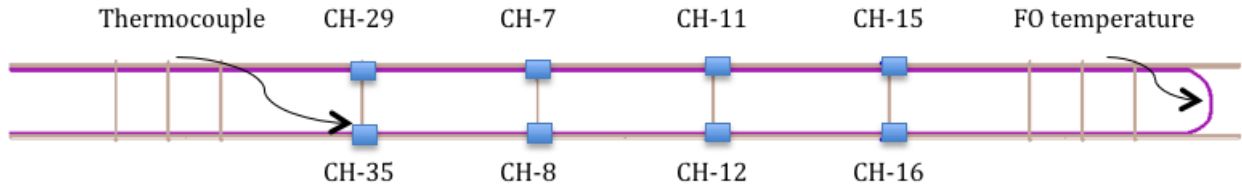


Figure 17 Locations of thermocouples for temperature measurements comparison

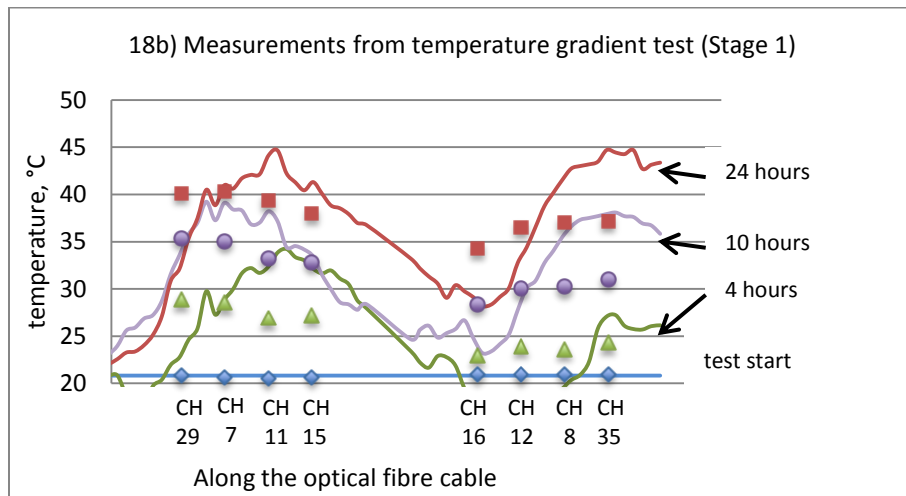
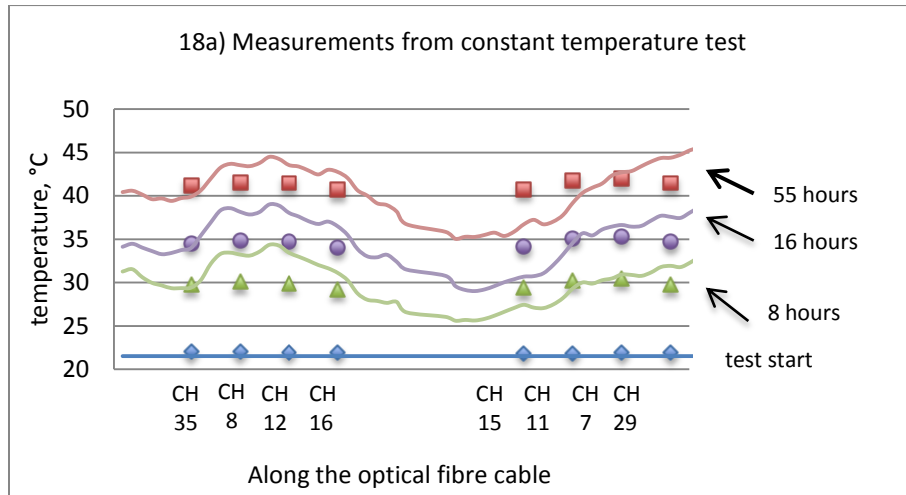


Figure 18 Comparison of temperature measurements from FO temperature cable and thermocouples

1
2
3
4 There are a number of methods used to conduct temperature compensation depending on the specifics
5 relating to the type of optical cable, optical fibre analyser and method of installation (Mohamad, 2012).
6
7

8
9 A loose-tube standard telecommunications cable (Unitube) was installed next to the Fujikura strain
10 sensing cable (JBT-03813) in order to conduct temperature compensation.
11
12

13
14 Mohamad (2012) showed that the thermal strain ($d\epsilon_{thermal}$) can be derived from the following
15 equation:
16
17

$$d\epsilon_{thermal} = (\alpha_a + \alpha_{jacket}) dT \quad \text{Equation 2}$$

18
19 where $\alpha_a = 19.47 \times 10^{-6} \text{m/m}^\circ\text{C}$ (BOTDR intrinsic thermal coefficient in a bare single-mode silica fibre)
20
21 and α_{jacket} is the thermal expansion coefficient of the fibre induced by the thermal stresses within the
22 jacketed optical fibres. When the optical fibre cable is fully embedded in concrete, the jacket thermal
23 expansion becomes less important as the concrete dominates and hence α_{jacket} can be replaced by
24 $\alpha_{concrete}$ the thermal expansion coefficient of concrete (Mohamad et al, 2014). The thermal strain can
25 then be subtracted from the total strain measured by the BOTDR analyser. For temperature
26 compensation of distributed strain fibre optical measurements, two commonly used data processing
27 methods are compared in this paper:
28
29
30
31
32
33
34
35
36
37
38
39

- 40 1) Subtracting the thermal strain from the total strain on a point by point ('pt to pt') basis along
41 the sensing length.
42
43
- 44 2) Averaging the thermal strain over a 1m length and then subtracting this value from the total
45 BOTDR measured strain over the same 1m length ('average 1m').
46
47
48
49
50
51

52 Figure 19 demonstrates the comparison of results from both experiments after compensating for
53 temperature effect with different methods. The 'middle' presents results obtained from the middle
54 strain cable which is barely embedded in concrete and 'side' means data from side cable that is attached
55 to reinforced steel bar as shown in Figure 1d. In the constant temperature experiment, for temperatures
56
57
58
59
60
61
62

1
2
3
4 beyond 33°C, strain measurements from both cables with either temperature compensation method are
5
6 giving close results with an average variation of less than 25µε. However, for temperatures between
7
8 20°C to 30°C, the result from side cable with “average 1m” temperature compensation methods shows a
9
10 particularly lower strain measurement. Correlated back to the temperature profile in Figure 6, the
11
12 specimen and fibre cable at this period of time were subjected to a rapidly temperature change
13
14 condition. Considering the operational characteristics of the BOTDR Analyser with the spatial resolution
15
16 of 0.5m and sensing time of ~30 seconds, the large variation in this part of the graph is within the
17
18 acceptable limits of the BOTDR.
19
20
21

22
23 Under a rapid temperature-changing environment, a larger variation in temperature results in a higher
24
25 uncertainty in thermal strain measurements and thus a different observation is made from the
26
27 temperature gradient test. As shown in Figure 19b, the linearity of the measured strain to temperature
28
29 graph is reduced, which implies that the material that the cable was attached to is the main factor
30
31 influencing the final results in this case. This is further confirmed by measurements from bottom part of
32
33 the beam: a better coherence is observed between results obtained from the two temperature
34
35 compensation methods at this level while a clear difference appears between results from the middle
36
37 cable and side cable.
38
39
40

41
42 Therefore, under a constant temperature condition where the concrete is gradually heated up, whether
43
44 to install the FO cable to reinforcement or barely in concrete will give insignificant difference in final
45
46 measurements. Alternatively, for situations where heat is quickly conducted through the concrete, the
47
48 material that the FO cable is attached to has a significant contribution to the final measurements. The
49
50 temperature compensation methods are found to have minor effect on either cable in either situation.
51
52
53
54
55
56
57
58
59
60
61
62
63
64
65

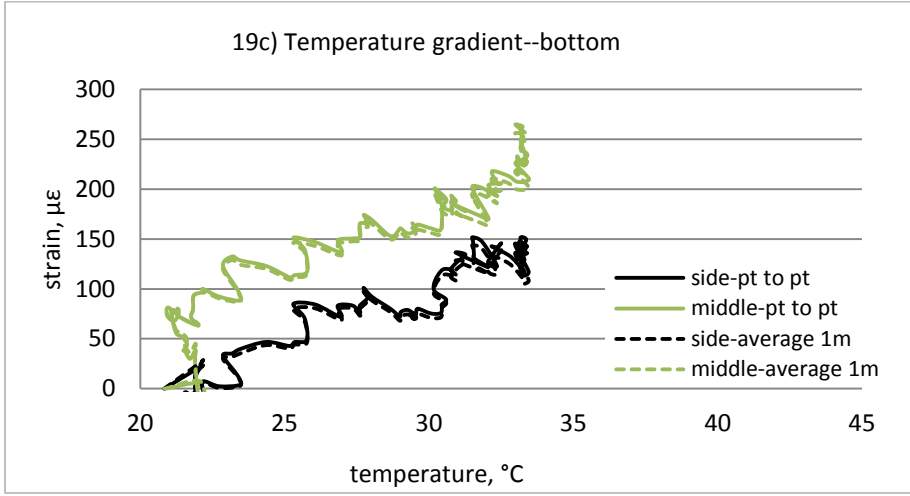
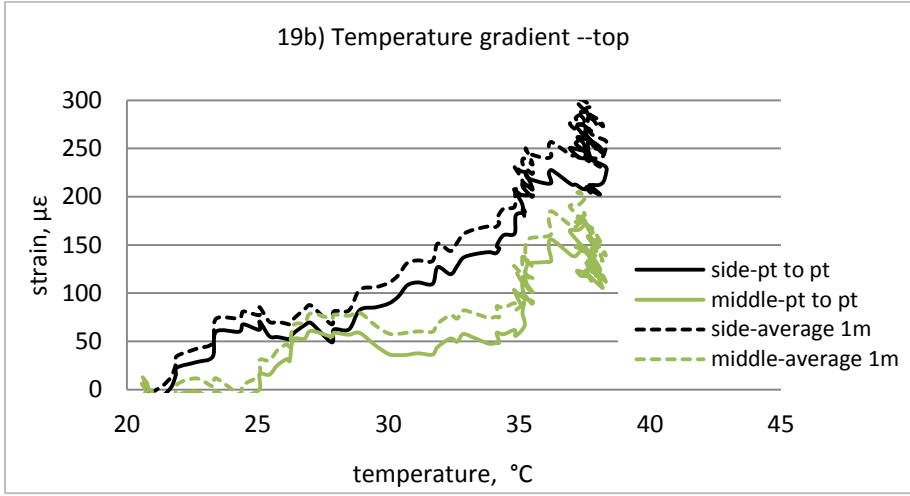
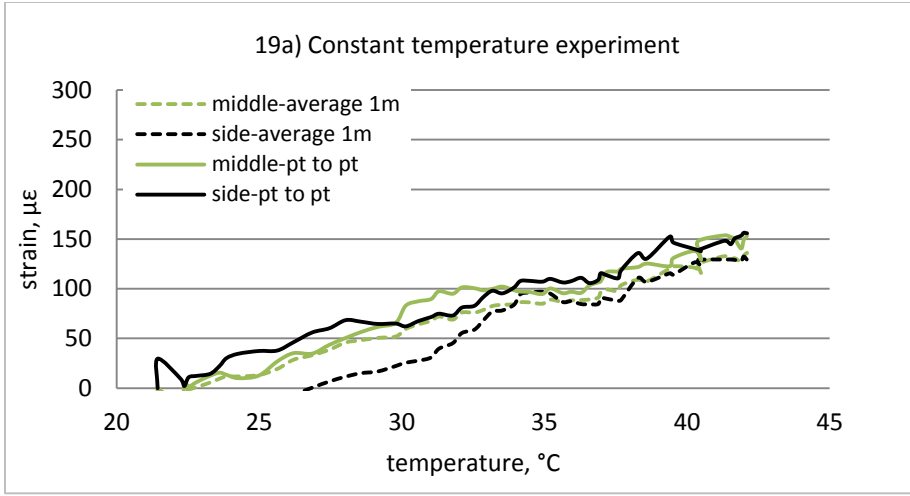


Figure 19 FO strain measurements after filtered (temperature compensated)

5. Conclusions

Civil engineering infrastructures, including bridges, buildings, pipelines, etc., begin to deteriorate once they are built and operated. They could also be subjected to unexpected loading scenarios and/or frequent changes in the environmental conditions. The importance of monitoring the health of these civil infrastructures over time cannot be overstated; maintaining safe and fully functional civil infrastructures for daily use is vital for the well being of all societies. A wide range of commercially available strain sensors are frequently used to record the performance of civil engineering structures with time and/or loading; however, a common problem faced when using these sensors is to distinguish strain changes experienced by the structure due to a temperature change from strain changes that occur due to other causes.

In this research, four types of strain sensors including (i) electrical resistance strain gauges (ERSs), (ii) vibrating wire strain gauges (VWSGs), (iii) Fibre Bragg Gratings (FBGs), and (iv) distributed fibre optic strain sensors (FO) were embedded inside a reinforced concrete beam to test their performance under thermal loading. The thermal loading included a constant temperature test where the whole beam was subjected to temperature change and a temperature gradient test where only the top surface of the beam was subjected to increasing temperature while the bottom surface was exposed to room temperature.

Comparison of the results that included compensation for temperature effects by following the guidance from sensor manufacturers demonstrated an average of 25% variation in measurements between the different types of sensors under the constant temperature test. For the temperature gradient test, an even larger variation (30%) in measurements was observed.

1
2
3
4
5
6
7 Correctly understanding the characteristics of the different sensors would significantly increase the
8
9 confidence in the measurements obtained; based on results obtained from the test reported in this
10
11 paper, the VWSGs produced the most stable and reliable results (compared to the theoretical
12
13 calculations) among the four sensors. It was demonstrated that the measurements from the FBG
14
15 sensors could show a significant amount of variation, which could be reduced substantially by calibrating
16
17 each individual sensor separately before installation and following strict installation procedures. The
18
19 paper demonstrated that ERSs could be highly unreliable due to their high sensitivity to the test
20
21 environment (ie, the installation surface and the covering material); this raises questions about their
22
23 long term monitoring viability inside concrete structures.
24
25
26
27
28
29

30 The FO sensors, with the advantage of providing continuous temperature or strain profiles, were unable
31
32 to give highly accurate temperature measurements inside concrete. In particular, a 5°C difference was
33
34 observed under a dynamic temperature environment. Thermocouples, in contrast, were highly reliable
35
36 in comparison; however a large number of thermocouples would be required to monitor large concrete
37
38 structures in practice with a much higher demand for labour during installation and cable routing.
39
40 However, for more stable thermal conditions where the temperature does not change quickly over short
41
42 periods of time, the continuity of the FO sensing provides a major advantage. The inability of FO sensors
43
44 to detect localised deformation due to the spatial resolution limitation can be overcome by using
45
46 properly calibrated VWSGs or FBG sensors where required.
47
48
49
50
51
52
53
54
55
56
57
58
59
60
61
62
63
64
65

Acknowledgement

The authors would like to acknowledge Dr. Peter Long, Martin Touhey and the Engineering Structures Laboratory technical staff at University of Cambridge for their assistance through the experimental program. The authors are also grateful to the Cambridge Center for Smart Infrastructure and Construction for supporting this research project.

References

- Bao, X. and Chen, L. (2011). Recent Progress in Brillouin Scattering Based Fiber Sensors, *Sensors* 2011, 11(4), 4152–4187.
- Chen, B., Maher, M.H., and Nawy, E.G. (1994). Fiber-optic Bragg Grating Sensor for Nondestructive Evaluation of Composite Beams, *ASCE Journal of Structural Engineering*, 120 (12), 3456–3470.
- Geokon Incorporation (2013). Instruction Manual, Model 4200 Series, Vibrating Wire Strain Gauges, <http://www.geokon.com> (accessed on 23rd/05/2013).
- Hoult, N.A., Bennett, P.J., Middleton, C.R. and Soga, K. (2009). Distributed Fibre Optic Strain Measurements for Pervasive Monitoring of Civil Infrastructure, *Proceedings of the 4th International Conference on Structural Health Monitoring of Intelligent Infrastructure (SHMII-4)*, edited by Urs Meier, Bernadette Havranek and Masoud Motavalli, 22nd-24th July 2009, Zurich, Switzerland; ISBN: 978-3-905594-52-2.
- Kreuze, M. (2013). Strain Measurement with Fiber Bragg Grating Sensors, Report Number S2338-1.en, HBM GmbH, PO Box 100151, D-64201, Darmstadt, Germany.
- Mohamad, H. (2012). Temperature and Strain Sensing Techniques Using Brillouin Optical Time Domain Reflectometry, *Proceedings of SPIE, Smart Sensor Phenomena, Technology, Networks, and Systems Integration 2012*, edited by T. E. Matikas, K. J. Peters, and W. Ecke., San Diego, California, 11th March 2012, vol. 8346,1-13.
- Mohamad, H. (2008). Distributed Optical Fibre Strain Sensing of Geotechnical Structures, Ph.D. Thesis, Cambridge University Engineering Department, United Kingdom.
- Mohamad, H., Soga, K. and Amataya, B. (2014). Thermal strain sensing of concrete piles using Brillouin optical time domain reflectometry, *ASTM Geotechnical Testing Journal*, vol 37, Issue 2 March 2014, 333-346.
- Neild, S.A., Williams, M.S. and McFadden, P.D. (2005). Development of a Vibrating Wire Strain Gauge for Measuring Small Strains in Concrete Beams, *Strain* 2005, volume 41 (1), 3–9.
- Neville, A. M. (1997). *Properties of Concrete*, Prentice Hall (publishers), 378-384, ISBN 9780470235270.
- Othonos, A. and Kalli, K. (1999). *Fiber Bragg Gratings: Fundamentals and Applications in Telecommunications and Sensing*. Artech House (publishers), 98-99, ISBN 9780890063446.
- Schwamb T. (2010). Optical Strain Sensing for Piled Foundations at Ninewell's Bridge, M.Phil. thesis, Cambridge University Engineering Department, United Kingdom.

1
2
3
4
5
6
7
8
9
10
11
12
13
14
15
16
17
18
19
20
21
22
23
24
25
26
27
28
29
30
31
32
33
34
35
36
37
38
39
40
41
42
43
44
45
46
47
48
49
50
51
52
53
54
55
56
57
58
59
60
61
62
63
64
65

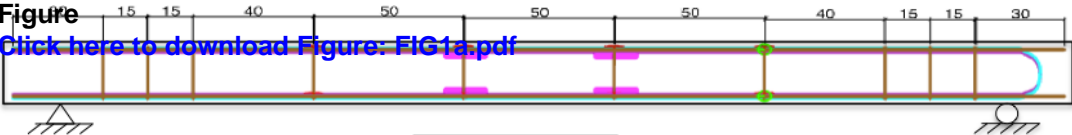
Sreeshyarn, P., Ravisankar, K., Parivallal, S., Kesavan, K. and Sridhar, S. (2008). Condition Monitoring of Prestressed Concrete Structures Using Vibrating Wire Sensors, International Journal of COMADEM, 11(3), July 2008, 46-54.

Webb, G.T. (2010) Structural Health Monitoring of Bridges, Fourth-year Masters project report, Cambridge University Engineering Department, United Kingdom.

Webb, G.T. (2011). Structural Health Monitoring, First Year PH.D. Report, Cambridge University Engineering Department, United Kingdom.4

Figure

[Click here to download Figure: FIG1a.pdf](#)

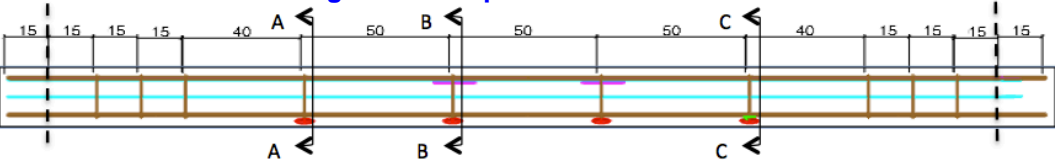


a) Elevation View

Figure
Centre line of
the support

[Click here to download Figure: FIG1b.pdf](#)

Centre line of
the support



b) Top View

Figure
[Click here to download Figure: FIG1c.pdf](#)







25
20

15
20

Section A-A

Section B-B

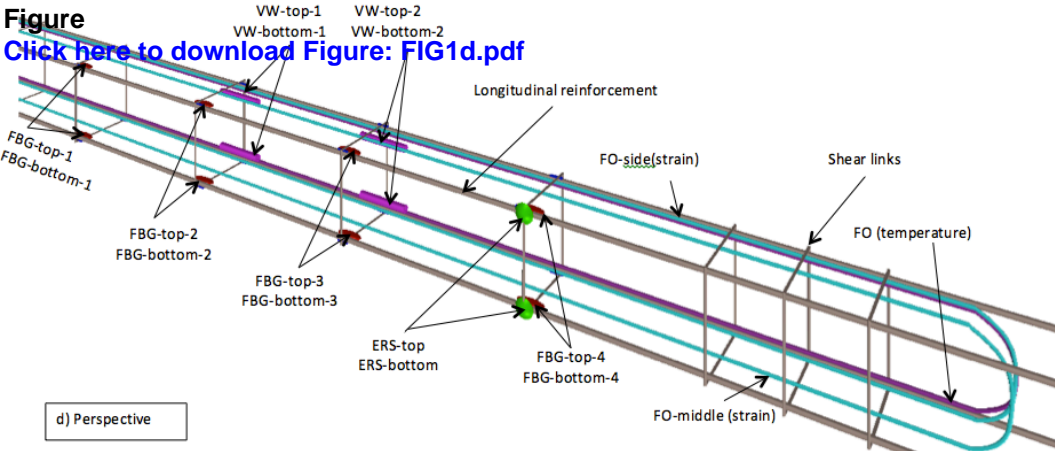
Section C-C

-  ERS
-  FBG
-  VWSG
-  Thermocouple
-  Optical fibre strain cable
-  Optical fibre temperature cable

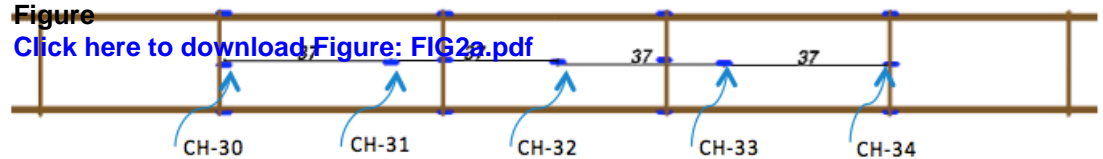
c) Cross sections of beam

Figure

[Click here to download Figure: FIG1d.pdf](#)



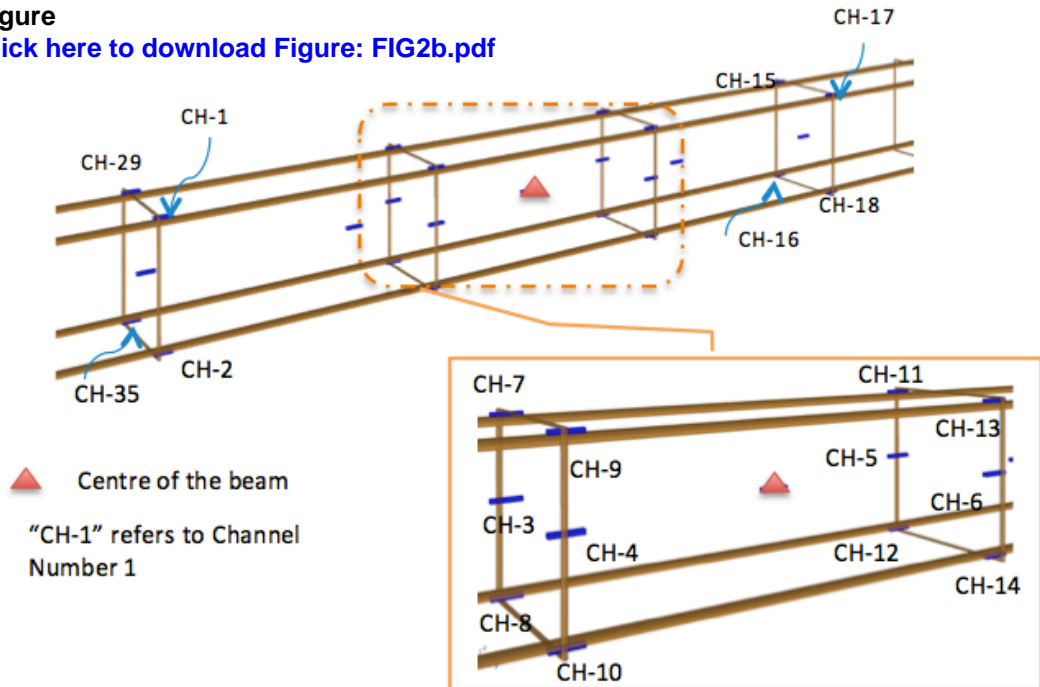
d) Perspective



a) Side elevation view of thermocouples locations (dimensions in 'cm')

Figure

[Click here to download Figure: FIG2b.pdf](#)

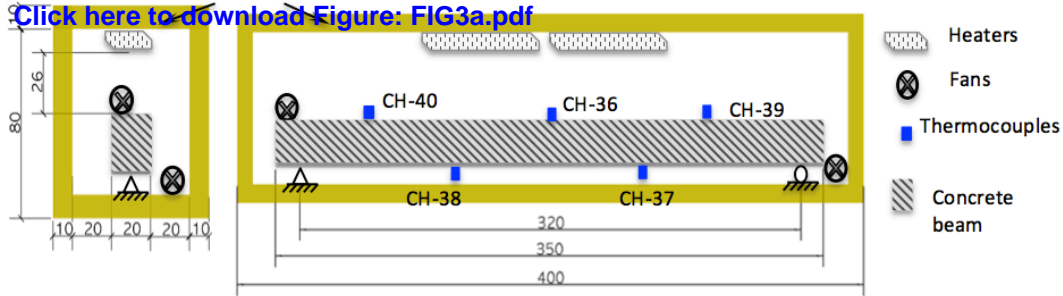


b) Perspective view of thermocouples

Figure

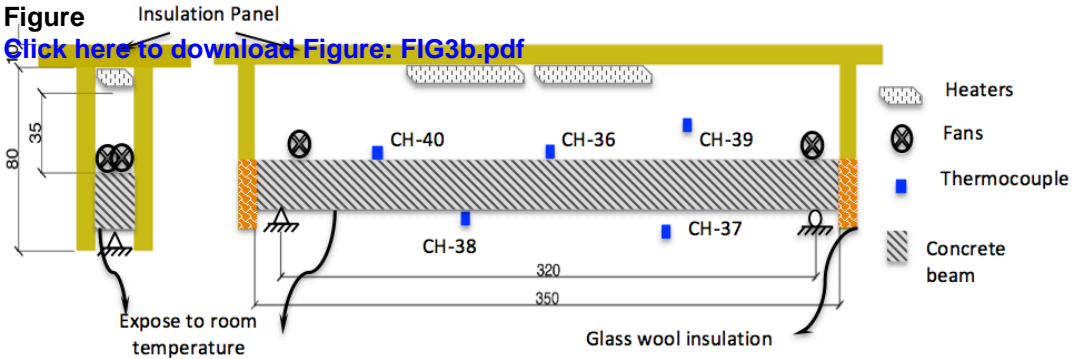
Insulation Panel

[Click here to download Figure: FIG3a.pdf](#)



a) The constant temperature experiment

Figure
[Click here to download Figure: FIG3b.pdf](#)

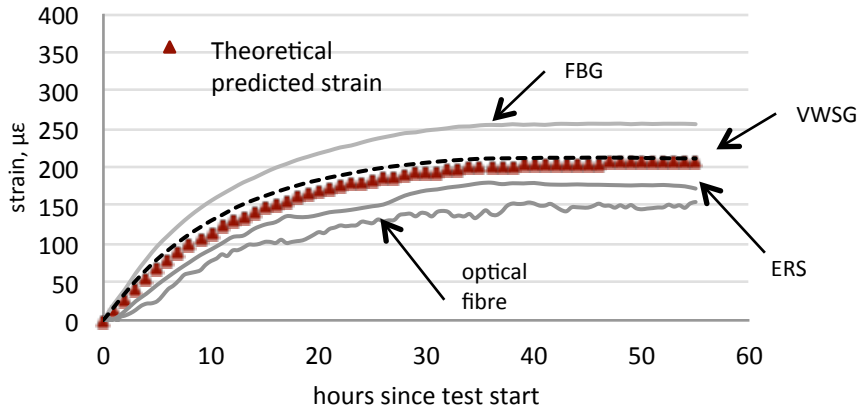


b) The temperature gradient experiment

Figure

[Click here to download Figure: FIG7e.pdf](#)

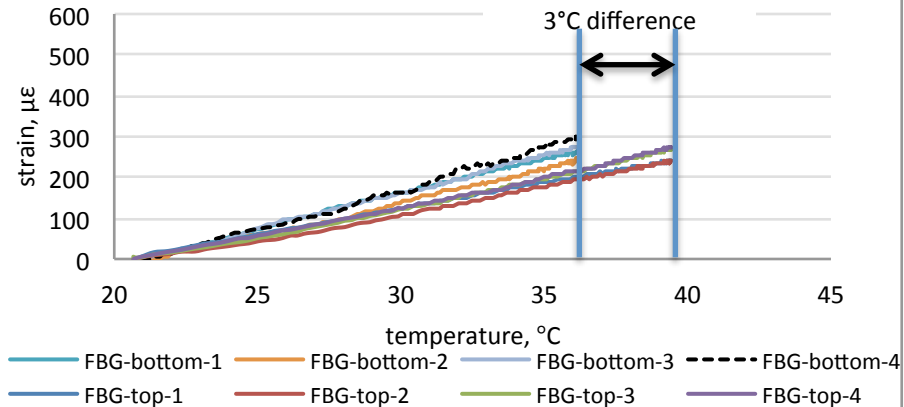
7e: Comparison of averaged results



Figure

[Click here to download Figure: FIG11.pdf](#)

FBG measurements after temperature compensation



Figure

[Click here to download Figure: FIG15.pdf](#)

VWSG measurements after temperature compensation

